

QuasarNet: A new research platform for the data-driven investigation of black holes

Priyamvada Natarajan^{a,*}, Kwok Sun Tang^b, Sadeh Khochfar^c, Brian Nord^{d,e,f}, Steinn Sigurdsson^g, Joe Tricotⁱ, Nico Cappelluti^h, Daniel Georgeⁱ, Jack Hidaryⁱ

^aDepartment of Astronomy, Yale University, New Haven, CT 06511, USA

^bDepartment of Astronomy, University of Illinois at Urbana-Champaign, Urbana, IL 61801 USA

^cInstitute for Astronomy & Royal Observatory, University of Edinburgh, Blackford Hill, Edinburgh, UK

^dFermi National Accelerator Laboratory, P.O. Box 500, Batavia, IL 60510, USA

^eKavli Institute for Cosmological Physics, University of Chicago, Chicago, IL 60637, USA

^fDepartment of Astronomy and Astrophysics, University of Chicago, IL 60637, USA

^gDepartment of Astronomy & Astrophysics and Institute for Gravitation and the Cosmos, Pennsylvania State University, 525 Davey Lab, University Park, PA 16802, USA

^hDepartment of Physics, University of Miami, Coral Gables, FL 33124, USA

ⁱSandbox@Alphabet, Mountain View, CA 94043, USA

Abstract

We present *QuasarNet*, a novel research platform that enables deployment of data-driven modeling techniques for the investigation of the properties of super-massive black holes. Black hole data sets — observations and simulations — have grown rapidly in the last decade in both complexity and abundance. However, our computational environments and tool sets have not matured commensurately to exhaust opportunities for discovery with these data. Our pilot study presented here is motivated by one of the fundamental open questions in understanding black hole formation and assembly across cosmic time - the nature of the black hole host galaxy and parent dark matter halo connection. To explore this, we combine and co-locate large, observational data sets of quasars, the high-redshift luminous population of accreting black holes, at $z \geq 3$ alongside simulated data spanning the same cosmic epochs in *QuasarNet*. We demonstrate the extraction of the properties of observed quasars and their putative dark matter parent halos that permit studying their association and correspondence. In this paper, we describe the design, implementation, and operation of the publicly queryable *QuasarNet* database and provide examples of query types and visualizations that can be used to explore the data. Starting with data collated in *QuasarNet*, which will serve as training sets, we plan to utilize machine learning algorithms to predict properties of the as yet undetected, less luminous quasar population. To that ultimate goal, here we present the first key step in building the BH-galaxy-halo connection that underpins the formation and evolution of supermassive black holes. All the compiled data, codes and associated Jupyter notebooks are available on the public Google Kaggle Platform.

Keywords: High Redshift Quasars, Database, Black Hole, BigData, Machine Learning, Cosmological Simulations

1. INTRODUCTION & MOTIVATION

Observations suggest that most galaxies in the Universe host central super-massive black holes (SMBHs), yet these are among the most enigmatic astrophysical objects. SMBHs, once believed to play a marginal role in the formation and evolution of their host galaxies, are now known to play a pivotal role as they appear to modulate star formation in galaxies. Theoretical modeling at present successfully embeds and integrates black holes - their formation, growth, evolution and impact on their environments - into the larger framework of structure formation in the Universe. According to the standard cold dark matter driven paradigm for structure formation, dark matter halos drive the formation of galaxies which in turn are the sites for the seeding of black hole (BH) formation and their subsequent growth. This tripartite coupling reveals the existence of an underlying BH-galaxy-halo connection. Exploring the

*Corresponding author

Email address: priyamvada.natarajan@yale.edu (Priyamvada Natarajan)

Preprint submitted to Elsevier

March 1, 2025

interplay between these visible and dark components has motivated the integration of simulations with observational data that we present here as the novel database and platform *QuasarNet*.

The coupling between SMBHs and their host galaxies presents as empirical correlations between the BH mass and properties of galactic stellar populations (see for example in: Magorrian et al. (1998); Gebhardt et al. (2000); Ferrarese and Merritt (2000); Tremaine et al. (2002); Gültekin et al. (2009); Kormendy and Ho (2013); McConnell and Ma (2013); Heckman and Best (2014)). The origin of these correlations is unsettled at present. How and when they are established are open research questions, and two possibilities are under active consideration (Alexander and Hickox, 2012; Natarajan, 2014). These correlations are suspected to either arise from the initial conditions that govern the formation of BH seeds (Woods et al., 2019), or from the coupled mass assembly history of galaxies and their central SMBHs over cosmic time (Haehnelt et al., 1998; Natarajan et al., 2019). Discriminating between these alternatives and discerning the causal mechanisms that underlie these observed correlations is challenging. To address this fundamental question, data across multiple cosmic epochs is required, including at very high redshifts, where observations currently peter out. However, with the spate of planned new observational facilities and instruments expected to come online shortly both on the ground and in space, a deluge of data probing the earliest cosmic epochs will soon be available. Combining the inhomogeneous data from these various independent surveys will be a complex task. We construct *QuasarNet* as a convenient template platform for this consolidation. The compiled data and our associated codes and Jupyter notebooks are publicly available on the Google Kaggle Platform.¹

A broad data landscape — including numerical simulations and multi-wavelength, multi-epoch observations — has been critical for building models that have helped us understand the growth history of BHs and their host galaxies over cosmic time (e.g., Haehnelt et al., 1998; Alexander and Hickox, 2012; Volonteri, 2012; Natarajan, 2014; Storch-Bergmann and Schnorr-Müller, 2019). The problem of simulating BH growth in the full cosmological context is numerically challenging due to the disparate physical scales involved - ranging from Mpc scale gas-flows in the cosmic web down to pc-scale gas accretion onto the accreting SMBH. However, over the past two decades, there has been enormous progress with the inclusion of what are referred to as sub-grid models that encapsulate the relevant detailed physical processes that cannot be implemented in an ab-initio fashion in computations (c.f. Springel et al. (2005a); Dubois et al. (2012); Sijacki et al. (2015); Gaspari et al. (2020)). We foresee an unprecedented alignment between the sophistication of computational models and the quality and quantity of data on SMBHs and their environments. Therefore, a systematic, statistical study of SMBHs simultaneously leveraging observational and simulated data with a brand new suite of tools is urgently needed to enable science breakthroughs.

Instruments like the Hubble Space Telescope (HST) and surveys like the ground-based Sloan Digital Sky Survey (SDSS) have acquired data on more than half a million quasars. And their archives contain not only raw data (e.g., images and spectra), but also high-level, value-added, and science-ready products — often in the form of relational databases. All HST data are archived in the Mikulski Archive for Space Telescope (MAST) archive and SDSS data are released periodically and are currently publicly available on several online platforms — e.g., CyVerse² and the NOAO Data Lab³ — that include additional tools to investigate data in situ. In the near future, multiple new instruments and observational campaigns — e.g., the Vera Rubin Observatory (VRO, formerly LSST), the James Webb Space Telescope (JWST), and the Nancy Grace Roman Telescope (NGRST) — will all contribute significant amounts of new data to the already large banks used for the investigation of SMBHs and their galaxy hosts. Meanwhile, next-generation peta-scale simulations are also currently being developed to complement this observational deluge. These two kinds of data are not integrated at present, and our work aims to fill this important gap with *QuasarNet*. To optimally exploit these upcoming data-sets, we propose methodologies for combined analysis of simulations and observational data that can deploy powerful, new tools tailored for the upcoming data rich era.

Machine learning (ML) methodologies are the natural set of go-to tools that we advocate for extracting maximal information from these varied data. In astronomy, which has always been a "big-data" science, ML is currently being vigorously explored to develop new analysis frameworks for many of the cutting-edge open questions. For example, in recently reported breakthrough work, the Event Horizon Telescope (EHT) collaboration relied on data from multiple wavelengths and ML methods extensively to generate the

¹www.kaggle.com/dataset/c09851833fc83fe549baa58d6fcc7fd9977d256876da943b5793d4c72ae92983

²<https://www.cyverse.org/>

³<https://datalab.noao.edu/>

silhouette of the SMBH at the center of M87 (Event Horizon Telescope Collaboration et al., 2019a,b). ML has demonstrated successes in a number of astrophysics applications (Ntampaka et al., 2019) — including image classification wherein convolutional neural networks (CNNs) have been used to morphologically classify galaxies and extract relevant properties from large observed samples (Ghosh et al., 2020); and Generative Adversarial Networks (GANs) have been used to recover features in galaxy images beyond the deconvolution limit (Schawinski et al., 2017). And in simulations, trained ML algorithms have been used to successfully (i) generate approximate dark-matter only cosmological simulations (He et al., 2019); (ii) predict and mimic a full hydrodynamic cosmological simulation (Kamdar et al., 2016); (iii) obtain new insights into cosmological structure formation (Lucie-Smith et al., 2020); including predictions of the evolution of angular momentum in simulations (Cadiou et al., 2020). The current generation of SMBH data already contain sufficient complexity that new ML algorithms are being developed and implemented for searches of accreting BHs and the analysis of their host galaxies. A natural extension of galaxy-halo connection studies is the incorporation of central SMBHs in galaxies with their parent dark matter haloes to illuminate the more fundamental underlying BH-galaxy-halo connection. This is the scientific question that has motivated us to develop *QuasarNet* and design the analysis tools presented here. It is clear that ML techniques are extremely powerful and could help unlock a deeper understanding with next-generation data sets, that will be more complex and larger. ML helps comprehend complex data and phenomena, and in turn, complex data sets benefit from highly flexible modeling frameworks, like ML. The power and prospects of insights gleaned by using ML in Astronomy more broadly have already been amply demonstrated (Moster et al., 2020; Bernardini et al., 2020; Dai and Seljak, 2020; Ntampaka et al., 2020). The BH formation and assembly problem is an example in which complex multi-faceted data will be a pillar for investigation. Determining causation for observed correlations to discern the underlying driving physical mechanisms is a key aspect of this problem. The challenges in understanding the causal relationship between BH properties and host galaxy properties suggest that more flexible algorithms and models may be needed. ML is yet to be used for the comprehensive and systematic study of SMBHs, a recent first attempt was made in deriving BH masses from spectral data (Yao-Yu Lin et al., 2020). Major stumbling blocks in the analysis of big data arises from the current limitations of ML techniques to discern between correlations and causal relationships and yielding predictive power beyond the training set. Models of astrophysical phenomena that are traditionally rooted in fundamental physical principles, uniquely enable mapping deeper correlations that can be related via causal chains. The BH growth problem offers an important test-bed to develop and hone new ML algorithms. However, there are additional known challenges that ML techniques more generally face, namely, in extrapolative prediction (Lucie-Smith et al., 2020); and in accurately quantifying uncertainties. For example, deep learning-based models lack native uncertainty quantification, which degrades their ability to make predictions beyond the data that they have seen (Lucie-Smith et al., 2020; Nord et al., 2019; Hortúa et al., 2020). Uncertainty quantification and biased models are topics of active research in deep learning, and are crucial to address to enable high-fidelity science.

In this paper, we describe *QuasarNet*, a new framework for the data-driven investigation of the underlying BH-galaxy-halo connection. To cope with the dramatic growth expected in the volume of available data on quasars and leverage these optimally for new discoveries, *QuasarNet* collates observational and simulated data and standardizes data in a user-friendly queryable database. In this pilot project, we focus on assembling all available optical data for the high-redshift ($z \geq 3$) quasar population for detailed study. At the highest redshifts, only the most luminous quasars are detected. Therefore, we have an incomplete and biased census of the BH population. Our goal is to develop tools that will help uncover the more characteristic, average quasars at these epochs, beyond the most extreme objects. We demonstrate that building the BH-galaxy-halo connection with *QuasarNet* will permit prediction of the properties of the more ubiquitous and more representative BH population at high redshift.

In what follows, we present the design and operation of the *QuasarNet* framework, built and tailored specifically to address the BH-galaxy-halo connection. We describe the landscape of BH data, observations collected from various astronomical surveys and simulations. The database design and the considerations taken into account to homogenize data in *QuasarNet* are discussed, as are illustrations of ease-of-use with concrete examples and visualizations.

We follow conventional notation, wherein accreting (actively evolving/growing) BHs detected in optical wavelengths are referred to as “quasars” (with luminosities $\sim 10^{15} L_{\odot}$) while those detected in X-ray observations are denoted as “AGN” (with lower luminosities ranging from $10^{10} L_{\odot}$ to $10^{15} L_{\odot}$). AGN are rare at $z \geq 3$, our chosen epochs for study in this pilot project, and the majority have identifiable optical quasar counter-parts. When referring to multi-wavelength data for accreting SMBHs, we use the term

AGN, and the term quasars when referring to optical data.

2. The BH-galaxy-halo connection

2.1. Co-evolution of galaxies and their black holes harbored in dark matter halos

All black holes - ranging from stellar mass to SMBHs - can be characterized by three fundamental properties: their mass, spin, and charge. This simplicity and small number of parameters needed to characterize BHs makes them attractive objects for systematic study. For astrophysical BHs, the subject of this work, charge is irrelevant, as they are expected to be charge-neutral (Znajek, 1977). Conceptual models of BH growth are therefore focused on their mass-assembly history and their spin evolution. We briefly describe the observed correlations that link central BHs to their host galaxy properties. The formation of galaxies is intricately coupled to the underlying properties of their parent dark matter halos, therefore, the existence of a galaxy-halo connection is well established. Our aim is to build new synthetic models that include BHs into this picture explicitly and extend this conceptual picture to understand the BH-galaxy-halo connection. Observations in the local universe reveal the existence of a correlation between the central SMBH and the stellar mass, luminosity, and velocity dispersion of stars in the inner regions (bulges) of their host galaxies (Ferrarese and Merritt, 2000; Magorrian et al., 1998; Tremaine et al., 2002; Häring and Rix, 2004; Gültekin et al., 2009; McConnell and Ma, 2013; Kormendy and Ho, 2013; Woo et al., 2015; Bentz and Manne-Nicholas, 2018; Sexton et al., 2019; Ding et al., 2020). These empirical correlations hold for local, inactive, dormant SMBHs over approximately five orders of magnitude in BH mass (from $10^5 - 10^{10} M_\odot$). At face value these correlations suggest that the assembly and growth of BHs is likely linked to the evolution of their host galaxies. These correlations could also reflect initial conditions, encoding the native properties of the sites where initial BH seeds form efficiently. One proposed channel for the formation of massive initial BH seeds from the direct collapse of pristine gas, naturally accounts for these correlations as an imprint of the initial seeding conditions (Lodato and Natarajan, 2006, 2007; Agarwal et al., 2014, 2019; Wise et al., 2019). Massive seeds have been invoked to account for the formation and assembly of the rare, most massive BHs. By contrast, light initial BH seeds appear to be sufficient to account for the more modest mass SMBHs with masses in the range of $10^6 - 10^8 M_\odot$, like the one harbored at the center of our own galaxy, the Milky Way. These measured local correlations may simply reflect the stochastic assembly process of galaxies via repeated merging (Peng, 2007; Jahnke and Macciò, 2011; Hirschmann et al., 2010; Ricarte and Natarajan, 2018a; Ricarte et al., 2019) over cosmic time. Therefore, understanding if these local correlations reflect deeper physical causes, astrophysical processes that self-regulate BH growth and star formation activity in a galactic nucleus is a question of fundamental importance. Whether such a correlation holds at earlier epochs for accreting BHs is not known at present Treister et al. (2011). More observational data are needed to probe if these correlations were imprinted during early cosmic epochs (Kormendy and Ho, 2013; Natarajan, 2014; Woods et al., 2019) and how and why they persist to late cosmic times. The differences between competing models of black hole growth are naturally more pronounced at early cosmic times (Ricarte and Natarajan, 2018b) as observational constraints at these epochs are sparser. Accessing data at these epochs has been a technical challenge, as distant accreting sources are significantly fainter. At high redshifts, we preferentially detect only the rare, highest luminosity quasars and the models have only this unrepresentative sample as guidance to predict properties of the more ubiquitous, and as yet undetected lower luminosity quasar population. For a more complete theoretical understanding we need comprehensive sampling of the entire range of luminosities and BH masses powering quasars and their associated hosts. Besides, we are yet to have detectors with the appropriate spectral sensitivity to capture emission from the early dusty universe, a situation that is expected to alter dramatically after the launch of JWST. Our pilot project targets these early epochs and aims to provide a framework for making predictions for the properties of accreting black holes that have lower luminosities than the currently detected population of high-redshift quasars. Our goal is to leverage *QuasarNet* by coupling simulations and observations in an innovative way and develop customized ML tools that will permit predicting the abundance and luminosities of quasars that are one to two orders of magnitude lower in luminosity than the brightest quasars currently observed.

3. METHODS

3.1. QuasarNet: Source Data

This section details the various sources from which data were collected and curated for *QuasarNet*. We create a comprehensive optical quasar repository that includes a combination of raw and high-

level products; covers a broad range of redshifts; and co-locates observational and simulated data of corresponding epochs - elements needed to construct extensive models of BH-galaxy-halo formation and co-evolution.

3.1.1. Observational Data

We used the NASA Extra-galactic Database (NED) to compile the quasar population data. Our primary data source NED, contains quasars retrieved from several independent optical surveys, principally the magnitude-limited Sloan Digital Sky Survey (SDSS). SDSS quasars have the most comprehensive data, quasars sourced from other surveys have much sparser spectroscopic and photometric information. While NED contains all quasars in principle, a population of high redshift quasars are missing due to being erroneously assigned lower photometric redshifts. The incorrect redshift assignment arises from a degeneracy in photometric redshift estimation methods. This is a well-known limitation of current photometric redshift determination methods (Salvato et al., 2019). The following procedure was used to construct tailored versions of the data for *QuasarNet*. First, we used the Astropy-affiliated package `astroquery` on NED to search and collect all known quasars at $z \geq 3$ from NED.⁴ In the next step, we used the `By Parameters` search query to collect all the basic information — object name, RA, DEC, redshift, photometry, spectra, images, and associated publication references — for each extracted object. Though NED itself takes duplications into account, we double-checked and performed a recursive search of the images, spectra, photometry, and reference tables associated with each object name to collate all the available data on a specific object that might originate from multiple independent surveys and catalogs. We have successfully culled duplicate entries arising from multiple assigned names for the same object. Prior to our work, quasars identified in high-redshift surveys were either recorded individually by their names or position in typical data-sets, which made it hard for researchers to query and cross-correlate properties. We have painstakingly assigned unique object identifiers while carefully removing duplications in *QuasarNet*. In this first level sweep in NED for $z \geq 3$ quasars, we know that there is a likely missing population due to incorrectly assigned lower photometrically derived redshifts; and possibly missing information due to NED not being fully updated.

To fill in the missing sources and accurately derive the entire $z \geq 3$ population of quasars, we moved directly to analyzing the published catalogs from all surveys. We scoured the tables and the accompanying Vizier catalogue sites⁵ for raw and derived properties of individual quasars. We collected object names, positions, redshifts, luminosities, masses, line-widths and Eddington ratios, when available. Instead of archiving only the reported BH mass, in *QuasarNet* we expand to include additional parameters used to derive the mass, like the line-widths, and luminosities. The raw quasar counts by redshift interval are shown in Table 1, and we note that there are source duplications, which are subsequently reconciled and filed under unique identifiers in *QuasarNet*.⁶ Our procured data and sources (their mass estimates) are summarized in Table 1 and the data is visualized in Fig. 9.

With several on-going observational searches for quasars, the data are rapidly evolving, and it is a real challenge to keep abreast and update databases with new finds. Besides, there are additional optical quasars detected in high-redshift surveys that are serendipitous finds. Luckily the overwhelming majority of accreting sources in our redshift range of interest are optical quasars so it is sufficient to track this population. The most recently reported detections are detailed in Kulkarni et al. (2019) and references therein. All these sources are now carefully checked and ingested into *QuasarNet*. For all the quasars that we have compiled, in various rest-frame M_{1450} wavelengths, we also include their detection probability which is based on their individual survey selection functions. We also record relevant survey specifications, information like the survey flux limits, redshift detection limits, sky area, survey magnitude limits for every detected source. This data is summarized in Table 2, and also shown schematically in Fig. 1. In Table 1, we list our compiled data for the $z \geq 3$ quasar population that includes available line-widths and luminosities from the published sources provided by NED (corresponding references are cited in the fifth column of the table). We note that not all quasars have data available to fill all entries. The incompleteness of recorded properties is reflected in the varying number of data points in the quasar property cross-correlation plots shown in Fig. 4. As BHs grow via gas accretion and by merging with other BHs, tracking both processes over time is integral to demographic modeling. Theoretical models of the assembly history of the BH population over time use two observationally derived functions as constraints:

⁴<https://ned.ipac.caltech.edu>

⁵<https://vizier.u-strasbg.fr/>

⁶Tables 1, 2 & 3 and Figures 6–10 can be found in the accompanying Supplementary Materials.

the Black Hole Mass Function (BHMF) and the Quasar Luminosity Function (QLF). The BHMF encodes the mass growth history as it is a statistical measure of the joint distribution of BH masses across redshifts. Similarly, the QLF is a statistical measure of the joint distribution of quasars in luminosity across redshift and reflects their accretion history. Both quantities evolve as functions of time in tandem in the back-drop of the corresponding mass build-up of the parent dark matter haloes. The QLF is a convolution of the BHMF and the Eddington ratio distribution, and was preferred for use by modelers as it is observationally well defined. For this pilot project focused on investigating the high redshift quasar population, we collate three tailored tables in *QuasarNet*— the **Quasar Spectra Table** that contains all available BH mass estimates; spectroscopic data like line-widths used for various independent BH mass estimators and errors therein when available, and quantities like accretion luminosities that also depend on the BH mass; the **Quasar Photometry Table** that contains all the available quasar photo-metric data measured across bands and the **Halo Properties Table** that includes the properties of the simulated putative parent dark matter halos for the corresponding redshift slices spanning $3 < z < 7$. In what follows, we briefly describe the process of assembling these and the challenges in doing so. All the collected quasar information was parsed to construct the Quasar Spectra Table and the Quasar Photometry Table as shown in Fig. 1. NED does not directly compile all available BH mass measurements. Using the observables listed in Table 1 we derive BH masses and Eddington ratios computed using the formalism outlined in the Supplementary Materials for inclusion in the Quasar Spectra Table in *QuasarNet*. To put together the Quasar Photometry Table, we include all available photo-metric data across bands for the sources. These are then used to construct QLFs. We demonstrate the use of *QuasarNet* to compute the QLF and the BHMF as test cases of the two key quantities needed to benchmark models of the assembly history of black holes over cosmic time. Though we have cross-checked and arrived at unique identifiers for each observed source, entries in Tables 1 and 2 do not completely overlap as not every source has all the attributes that we select for tabulation. To date, *QuasarNet* contains the most complete compilation of observed optical quasars — unique objects with data on all parameters that are available, as outlined in Table 1 & Table 2.

3.1.2. Simulation data

For this pilot project, we ingested simulated data from the LEGACY runs, a set of large-scale cosmological dark matter-only simulations (Khochfar et al. in prep.). We defer adding simulations that include baryons to the next stage of our project as we have focus here on the first step to derive ML tools that will permit the creation of mock simulation volumes that mimic observational survey volumes. This set of LEGACY simulations consists of a parent simulation with a $(2.3 \text{ Gpc})^3$ volume of 2048^3 particles at a mass resolution of $M_{\text{DM}} = 5.43 \times 10^{10} M_{\odot}$ which is accompanied by a set of zoom-in simulations with a volume of $(119 \text{ Mpc})^3$ and mass resolution of $M_{\text{DM}} = 1.32 \times 10^7 M_{\odot}$ and one further zoom-in simulation with $V = 1 \text{ Gpc}^3$ and $M_{\text{DM}} = 6.78 \times 10^9 M_{\odot}$. The initial conditions of the simulation are created using the public code MUSIC (Hahn and Abel, 2011), assuming the following values for cosmological parameters based on the results from the WMAP satellite (Hinshaw et al., 2013): $\Omega_{\Lambda} = 0.715$, $\Omega_{\text{M}} = 0.285$, $\Omega_{\text{b}} = 0.045$, $h = 0.695$, $\sigma_8 = 0.828$. For each of the simulations (parent and zoom-ins), we identified gravitationally bound structures and sub-structures using the halo finder ROCKSTAR (Behroozi et al., 2013).

Within the parent simulation, several regions of varying over-density are identified and re-simulated at higher resolution within the larger cosmic volume, permitting large-scale density fluctuations to affect the evolution of these re-simulated dark matter haloes (Klypin and Prada, 2019). Each of these regions has a volume of $(119 \text{ Mpc})^3$ and an increased (coarser) mass resolution of $M_{\text{DM}} = 1.32 \times 10^7 M_{\odot}$, which corresponds to an effective particle number count of 32768^3 . In addition, a larger zoom region of $(1 \text{ Gpc})^3$ at a mass resolution of $6.78 \times 10^9 M_{\odot}$ has also been simulated. Particles and halo/sub-halo properties have been stored in 300 snapshots between $z = 20$ and $z = 0$, covering the redshift range of interest in this study, namely, $z \geq 3$, though slices are available up to $z = 0$. The full LEGACY halo catalogs provide a multitude of detailed information - 81 attributes for each identified halo - and all of these characteristic parameters are stored in *QuasarNet*. A few examples of basic halo properties that we store are shown in Table 3 and in the schematic in Fig. 1 as the Halo Properties Table. The strategy we follow is to make all derived halo data available. In addition to the halo catalogs, which provide snapshots of the dark matter halo population, we also store detailed evolutionary information for each halo. Approximately 200 finely spaced time steps from $z = 20$ to $z = 0$ are used to generate merging histories for individual halos. The data structure allows us to identify for each halo its progenitors and ancestors in a unique way. This information provides further leverage in establishing links to evolutionary models and provides the

crucial BH-halo connection piece, to track BH growth in combination with observational data. *QuasarNet* permits the potential association of the host dark matter halo hierarchy for each observed quasar. This is one of drivers for our project as it is currently the missing piece in theoretical models needed to study the BH-galaxy-halo connection. These simulations combine sufficient spatial resolution to identify dark matter halos that would host SMBHs with the ability to follow their merging history back in time to test evolutionary models of black hole growth. Many new probes of host halo properties for SMBHs are available for tracking. For instance, in Fig. 2, we show the merger history of a SMBH-host halo, assuming that the brightest observed quasar at $z = 3$ is hosted by the most massive dark matter halo at $z = 3$. The host dark matter halo has a mass of $9.3 \times 10^{12} M_{\odot}$ and is amongst the most massive halos in the simulation volume at this redshift — thus, a likely candidate to host a SMBH.

The ultimate goal of this project is to make full use of the powerful capabilities of ML to analyze these complex multi-dimensional data sets together. To this end, we have combined simulation and observational data sets by epoch in *QuasarNet* which permits seamless application of ML techniques. The co-located simulated and observational quasar data-sets in *QuasarNet* enables us to create extended simulation volumes to mimic the footprint of observational surveys. The creation of such analogs permits easy splitting of the parent simulation into training and validation sets for ML applications. The range of halo properties that we have stored from simulations can easily be expanded to add more attributes for creating extended catalogs corresponding to galaxy surveys of varying depths and volumes. This will uniquely allow us to connect across data types and test against predictions for the occupation fraction and larger scale environments of the SMBH population.

4. RESULTS

4.1. *QuasarNet: Database Design, Structure and Development*

We describe the challenges of collecting and formatting multiple, independent sources of quasar data and how the *QuasarNet* structure addresses those challenges. The *QuasarNet* database tables are arranged by source identifiers — NED, individual observations, survey observations. Fig. 1 depicts a color-coded layout of the tables: blue boxes contain data sourced from NED; the red Quasar Spectra Table contains the properties of individual objects collected from other additional published sources (listed in Table 1; and the orange Quasar Photometry Table that includes all the selection functions collected from published targeted quasar surveys (listed in Table 2).

In the NED database, data for each object are stored individually in tabular form. While this format is ideal for in-depth study of each object individually, it is too cumbersome to perform statistical analyses or apply ML methods on the population as a whole that we seek to do. Modeling work typically relies on population studies and hence requires larger data samples as inputs. To address what we see as a fundamental incompatibility of format and availability with the current and future need for scientific research purposes, in *QuasarNet*, data attributes like the photometry, redshift, luminosity, references, downloaded with `astroquery` from NED are first flattened and combined into respective attribute tables. The schema and the structure of our database is shown in Fig 1. To construct a fully queryable database, we have associated and linked each of the entries to an individual unique quasar identifier. This is a critical first step as almost all of these objects typically come with multiple names and identifiers. A simple query that appends tables by name would be unsuccessful as entries that correspond to the same object may not be identified by the same name. In order to facilitate usage we have therefore unified the naming convention, based on the name identifier on the NED database. All object names were queried iteratively on the NED database with `astroquery.query_object`, and are replaced with the identifier from NED if they don't match the name reported in the catalog/literature.

The data table for Quasar Spectra properties is shown in Fig 1 in red. We follow the column naming convention in (Shen et al., 2011), where all the derived properties such as black hole mass `LOG_BH`, the luminosities `LOG_LBOL` are presented in log-scale in units of M_{\odot} and erg s^{-1} respectively. The line-width of various emission lines are presented in the units of km s^{-1} , and the Eddington ratio `LOG_EDD_RATIO`, which is dimensionless, is stored also in log units. And errors in these mass estimates, when available or when computable using the methods outlined in the Supplementary Materials, are also stored.

From the Quasar Photometry Table, we ensure that QLFs are reproducible from the database by including the selection function, ensuring that the effective surveyed volumes can be calculated independently for different cosmologies (with assumed values for the standard cosmological parameters) adopted in various published papers. One of the advantages of this comprehensive collation is that it permits flexible searches that can be indexed by a unique name, redshift, and luminosity along with

a uniform and well-defined metric for detectability. For the plots shown here, the values for standard cosmological parameters adopted are: $\Omega_m = 0.3$; $\Omega_\Lambda = 0.7$ and $H_0 = 70$ km/sec/Mpc. Our plan for *QuasarNet* is to continually compile and add new data when available into this standardized and uniform format for ease of use. In this pilot version, the tasks described above are done manually, however, it can be set up for automatic dynamic updating which we will set up in the next stage of our project.

4.2. Example: Querying the Database

To facilitate querying the database, searches can be performed with SQL-like BigQuery on Google Public Dataset on Kaggle.⁷ With the data hosted on the public Google Kaggle Platform, researchers can directly access and interact with the data through a Colab notebook that we provide and perform analyses directly on the dataset. The subset of photometry data for instance, can be accessed for all quasars given their names with the following query:

```
1 %%bigquery --project black hole-database df
2 SELECT
3 qtable.*,
4 ptable.*
5 FROM 'black hole-database.ml_test.qso' as qtable
6 JOIN 'black hole-database.ml_test.photometry' as ptable
7 ON qtable.object_name = ptable.source_object_name
```

The Quasar Spectra Table and the Quasar Photometry Table are stored similarly, therefore, simply replacing “qtable” with “qlftable” will yield the existing photometry data for all quasars across surveys.

4.3. Workflow Examples: Observational Data

Using the described workflow and sample queries, we demonstrate the ability to quickly compile a suite of essential information on SMBHs. Models of the mass build-up history of BHs over cosmic time can be described by the flux-limited BHMF at multiple redshifts. The space density of SMBHs can be estimated using measurements of BH masses and knowledge of the flux limit of the observations. In a given quasar survey (i.e. from Table 2) every detected quasar can be assigned a detection probability and a detection volume in a given redshift bin according to the relevant survey detection limit. The corresponding properties for the quasar can then be retrieved from Table 1, and combined with the spatial density information to derive an estimate of the QLF with Equations 4 and 5. Similar to the computation of the QLF in *QuasarNet*, we assign each quasar with an associated detectable volume estimate based on its luminosity and the respective survey sample completeness properties for deriving the BHMF. These are then binned in mass with weights inversely proportional to their detectable volume. To illustrate, in Fig. 10 we plot the BHMF obtained with the uniformly selected data set of SDSS DR7 (Willott et al. (2010a); Jiang et al. (2016)). Note that while the derived BHMF shown here is not corrected for survey incompleteness, this illustration provides a crude, but very swift way this key quantity. However, the mass completeness corrections can also be computed within *QuasarNet*. In earlier work by Kelly et al. (2010), the BHMF was derived from the SDSS DR3 data release, here we demonstrate the ease-of-use to generate the updated BHMF. Fig. 10 shows that, selection effects notwithstanding, there appears to be an upper limit for BH masses across redshift. Interestingly, this is theoretically predicted and this rendering of data compiled in *QuasarNet* aligns with expectations (per Eqn. 7 in Natarajan and Treister (2009)). The visualization of data garnered with the few sample queries discussed here are presented in Figs. 9, 3, 4, 10. In Fig. 3, we plot BH properties derived as a function of redshift from a sample query to *QuasarNet*. There is a precipitous decline in the number of quasars with redshift, this steep fall-off provides insights into the shape of the QLF and its slope as a function of redshift as well as selection functions that limit detectability of the faintest and most distant sources. At lower redshifts, $z < 2$, a similar decline in the abundance of quasars is seen, which does not reflect our ability to detect them but rather signals the true deficit of actively accreting BHs at these late times. The low redshift decline in the number of detected quasars is well understood, as at late times galactic nuclei are gas-poor with much of the gas already consumed by star-formation. The top panel of Fig. 3 shows that most of the detected quasars are accreting at sub-Eddington rates. This finding likely reflects the fact that we are missing the optically dim, dusty super-Eddington sources that are yet to be uncovered at these early epochs. We reiterate that *QuasarNet* includes all X-ray detected Type I AGN as well, since they all have optical quasar counter-parts. Given the current limits of X-ray instruments on the Chandra telescope and XMM-Newton telescope, accreting

⁷www.kaggle.com/dataset/c09851833fc83fe549baa58d6fcc7fd9977d256876da943b5793d4c72ae92983

sources peter out at $z > 3$ where Type II AGN inventory is expected to increase. This is where we expect JWST and NGRST to start filling in the landscape. Current observational techniques detect progressively brighter quasars at high redshifts. Reading off the peaks of the contour plots in Fig. 3, the bolometric luminosity of the average detected quasar at $z = 3$ is $3.6 \times 10^{46} \text{ erg s}^{-1}$, while by $z = 4$ it is an order of magnitude higher at $2.8 \times 10^{47} \text{ erg s}^{-1}$. Meanwhile, the typical measured BH mass powering the corresponding average detected quasar exceeds $10^9 M_\odot$ at all $z > 3$. This demonstrates clearly that we sample different sub-portions of the QLF and BHMF as a function of redshift, and preferentially access the most extreme objects at earlier epochs. This observational selection severely limits our ability to model the growth history of the overall BH population. This is our over-arching goal with *QuasarNet*, to combine current observations with simulations and leverage ML to predict properties of the as-yet undetected lower luminosity quasar population and their galaxy hosts. *QuasarNet* will provide insights into observational strategies and new selection methods to detect the larger population of quasars, yielding a more complete picture of BH growth and galaxy assembly. Next, Fig. 4 demonstrates the ease of visualizing the data and exploring correlations between measured quantities relevant to BHs. Several interesting science results emerge from just this single analysis. For example, the second panel on the bottom row clearly shows an anti-correlation between the FWHM of CIV lines versus Eddington ratio. In a recent paper, Marziani et al. (2019) report the same and discuss that a correction needs to be applied to the FWHM of CIV derived BH masses that depends on the Eddington ratio for a lower redshift population of quasars $0 < z < 3$. Our plot suggests that this trend extends to higher redshift quasars at $z > 3$ studied here. With these examples we illustrate the power of *QuasarNet* to reveal new correlations and their evolution as seen in the diagonal kernel density plots as a function of cosmic epoch.

4.4. Workflow Example: Probing Properties of Halo Distributions with Simulation Data

Next, we use simulations to explore the connection between BHs, galaxies, and their dark matter haloes in *QuasarNet*. In *QuasarNet* these simulated dark matter halo attributes are stored in the Halo Properties Table as shown in Fig. 1. In this section, we show how these properties can be used to learn more about the underlying non-parametric distributions for halo characteristics that will enable the efficient generation of new/unseen halo data. This is an important first step needed to circumvent the simulation volume limits as our goal is to perform spatial association studies with the observed rare quasar population. And this is where we unleash the power of ML techniques and tools. We demonstrate the potential extraction and analysis of halo attributes from the wealth of simulated data available in *QuasarNet*. We characterize ensemble properties of this data and use them to extend and derive putative properties of the overall halo population, in order to generate dark matter halos that are not available in our simulation volume. For the purposes of illustration, the statistical properties of the underlying dark matter halo population are derived using the class of generative machine learning models referred to as normalizing flows (Rezende and Mohamed, 2016). In normalizing flows, the observed variables X , in our case, the properties of each halo such as its mass, angular momentum (modeled via its spin parameter), mass accretion redshift (redshift at which half the mass of the halo is assembled) etc, are mapped to a latent variable $z \sim p_z(z)$ of the same dimension drawn from a known distribution (usually Gaussian) through an invertible transformation parameterized by a neural network, i.e. $z = f_\theta(X)$. The marginal likelihood of $p(X)$ can be obtained with the changes of variables given by:

$$p_X(X; \theta) = p_z \left| \det \frac{\partial z}{\partial x} \right| = p_z(f_\theta^{-1}(x)) \left| \det \left(\frac{\partial f_\theta^{-1}(x)}{\partial x} \right) \right|. \quad (1)$$

The model is trained by maximizing the log likelihood of the estimate under the observed sample distribution X . Once trained, the model can generate data by sampling the latent (z') space from the base distribution and transforming it through the invertible transform $X' = f_\theta^{-1}(z')$. Unlike typical neural networks, normalizing flows are restricted to the class of bijective transformations that are exactly invertible. Several other kinds of transformations have been proposed (Dinh et al., 2017; Kingma et al., 2017; Papamakarios et al., 2018). Here we choose normalizing flows as it is particularly well attuned to deriving the probability distributions from which larger volume statistics for the halo population can be generated for our planned association studies. Normalizing flows also offer a flexible way of modeling the joint data distribution in the multi-dimensional halo properties space. Applications of normalizing flows in astronomy have been shown to successfully constrain the posterior estimate of the distance estimates from Gaia Data (Cranmer et al., 2019), performing likelihood free Bayesian inference on the cosmological parameters (Alsing et al., 2019) and in constraining the re-ionization history of the universe (Hortúa et al., 2020). Preliminary results of this crucial first step in the combined exploitation of simulated and

observed data are shown in Fig. 5. We adopted the Real Non-Volume Preserving model (RealNVP) (Dinh et al., 2017) to fit our simulated halo properties tables. The generated host dark matter halo population is distributed similar to the true halo population stored in the Halo Properties Table from the LEGACY cosmological simulations slices in *QuasarNet*. This first step enables efficient sampling from the trained model which can then be used further for downstream ML tasks that will explicitly explore the quasar - host halo connection. The use of normalizing flows permits us to extend our simulated catalog to generate the rarer dark matter halos that would only appear in significantly larger volume simulations.

4.5. Discussion & Future Prospects

In this paper, we develop a new research platform *QuasarNet* that comprises co-located observational and simulated data for the study of the growth and assembly history of black holes over cosmic time. With this pilot project, we demonstrate that the deeper connection between black holes, their host galaxies and parent dark matter halos needs to be and can be studied in order to fully understand how black hole growth unfolds in the larger cosmological context of structure formation. We present the first collated database of high-redshift optical quasars in a format ready for application with ML techniques. Offering homogenized data from many disparate observational surveys, we also make available detailed information and properties where available for individual objects tailored to address the problem of understanding the growth and assembly history of the earliest black holes at $z > 3$. Our framework is integrated with simulated data from the LEGACY simulation. While full exploration of the BH-galaxy-halo connection with further customized ML tools will be pursued in follow-up work, here we present *QuasarNet* and how to query it to derive key properties of interest. We show how the explicit association of observed quasars at $z \geq 3$ with their putative parent dark matter halo sites and their history can be used for improved modeling. Given that quasars are rare objects, in order to circumvent the limitations of the simulated box size for our planned association studies, we present a ML enabled way using normalizing flow to expand our sample of simulated halo catalogs. Using normalizing flow, we illustrate that we can derive the underlying parent distributions for the stored properties of simulated dark matter haloes in *QuasarNet* and draw from these distributions to generate simulated volumes that correspond to observational survey volumes. While the data collection and updating for *QuasarNet* is currently done manually, with this flexible database in place, we plan to deploy ML techniques and natural language processing to look for new (continually dynamically update from on-going surveys for instance) as well as any missing quasar data. By computing the semantic similarity of the subset of literature we currently include in our database with the rest of the references from NED, we can obtain a list of relevant references that have been potentially missed, and hence expand the coverage of our database.

We have crafted the pilot project to focus on best available data at the moment - the highest redshift optically bright quasars that correspond to the Type I AGN population. Obscured accreting sources, Type II AGN data are much more sparsely detected at $z \geq 3$, though they are expected to exist more abundantly. As future infra-red and X-ray surveys start to reveal this heavily obscured high- z population, the inherent flexibility in the database structure of *QuasarNet* would permit seamless addition of these sources. Meanwhile, with our current approach, we aim to provide insights into optimal detection strategies for the lower luminosity quasars at $3 < z < 7$ to fill in the current gaps in our knowledge of this population. Our hope is to leverage these current tools, build upon them further ML to predict the properties of this as yet undetected quasar population. Spectra contain significantly more information than photometry and are therefore the goal of many observational surveys. Spectra and images are often in the form of FITS files. While the FITS file format is good for storing meta-data related to the observations, it is sub-optimal for large-scale cross-correlation studies between objects in a common ML framework. We currently do not actively store imaging data in FITS format in *QuasarNet*. In future efforts homogenizing these kind of data, finding a good and optimal embedding representation of these data would be extremely beneficial to advance the use of structured ML based studies.

In this paper, we describe the assembling of the *QuasarNet* platform and demonstrate a few of its powerful capabilities for the combined multi-dimensional studies that will permit us to associate observational data of quasars with potential formation sites and their properties in corresponding time-slices of simulated data. In follow-up work, we plan to explore the interplay between observations and simulations and explore predictions for undetected quasar populations and their properties using ML algorithms.

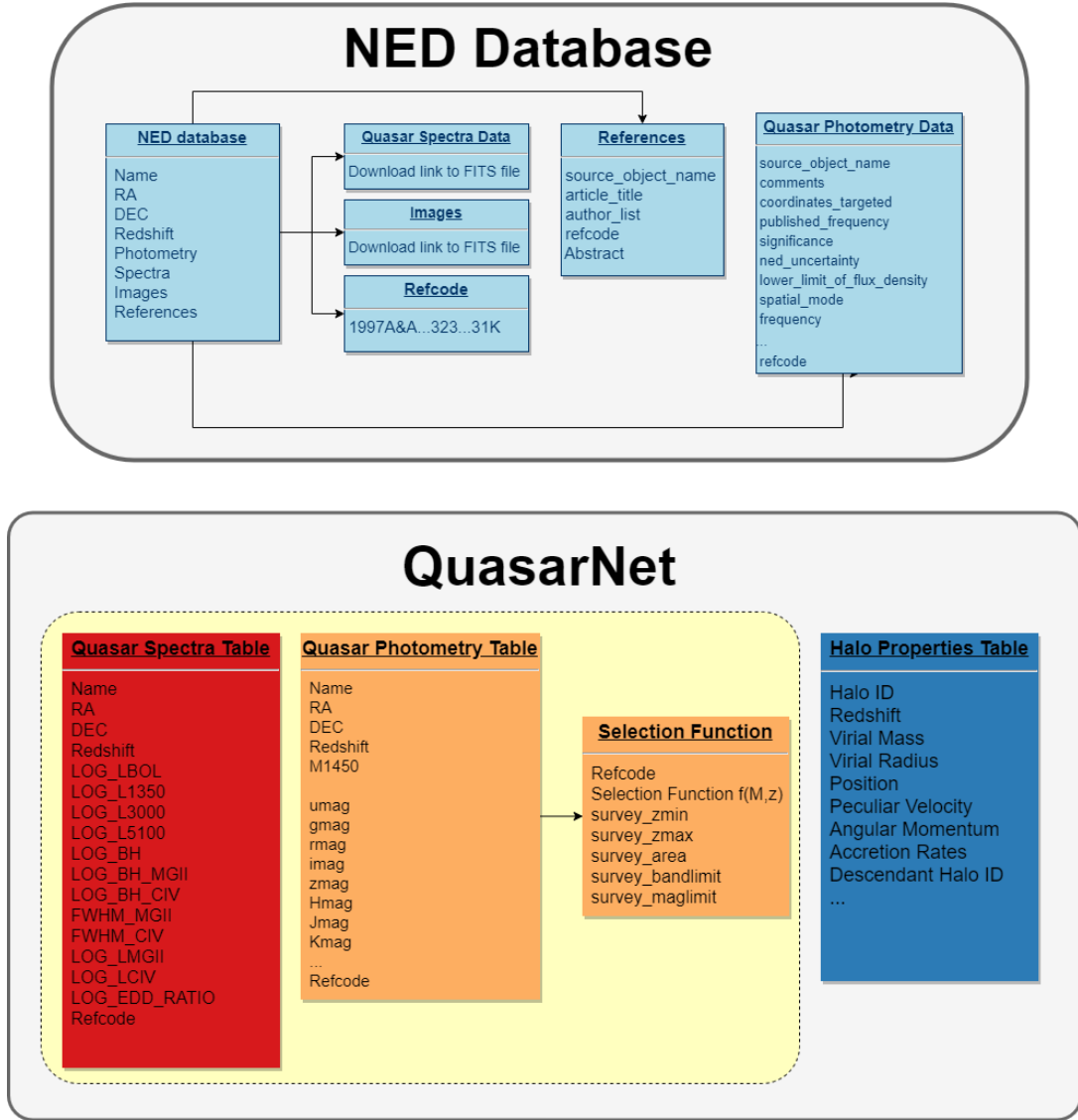


Figure 1: Schematic of the data structures and derived custom data tables that comprise *QuasarNet*: Information sourced from NED and following up references therein is shown in blue; the collated data in the Quasar Spectra Table that will be used to generate the BHMF are shown in red; the Quasar Photometry data table that will be used to determine the QLFs is in orange and the data table for Halo Properties derived from the simulated LEGACY catalogs is shown in blue. In *QuasarNet*, we assign unique identifiers, and any quasar duplications across the two custom data tables have been removed using the object name, RA, and DEC fields. The Quasar Spectra table contains the collated measurements of the luminosity, redshift, and BH masses reported in the literature. Additional measurements such as line-widths and luminosity proxies are also included to derive BH masses, which can be updated using newly calibrated virial mass relations, if needed, and when available. The Quasar Photometry data table contains a compilation of optical quasars from various high redshift campaigns targeted to derive QLFs, that includes magnitudes; survey specifications for each source; survey areas; flux limits and selection functions, which are all stored.

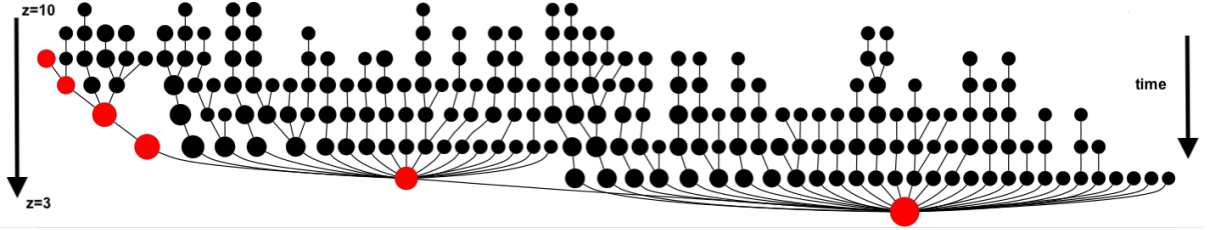


Figure 2: Dark Matter Halo Population Demographics: The merger and assembly history of a dark matter halo that hosts the brightest observed quasar at $z = 3$ tracked through time. This merger tree structure reflects the assumed association prior - that the most massive BH is hosted in the most massive dark matter halo. The size of the circle is proportional to the logarithm of the dark matter halo mass. Red circles delineate the most massive progenitor of a halo at each time step. Halos grow hierarchically in mass through a sequence of repeated merger events and by the accretion of less massive halos. Here we only show progenitors with mass $\geq 5 \times 10^9 M_{\odot}$ and only time steps with $\Delta z \sim 1$.

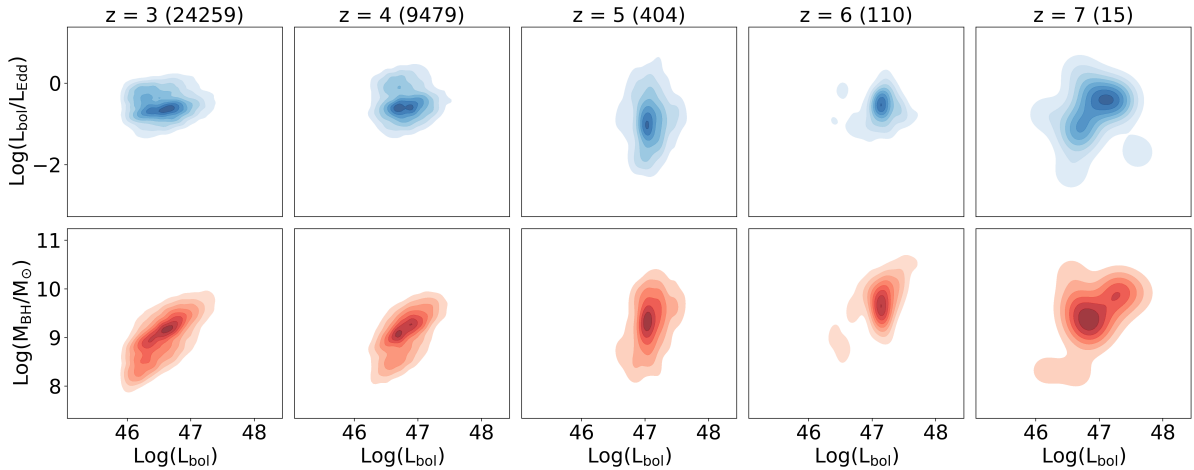


Figure 3: Key derived statistical properties of the population of observed $z \geq 3$ quasars relevant to modeling their growth history over cosmic time - black hole mass, bolometric luminosity and Eddington ratio - in 5 redshift slices. The number in parentheses denotes the number of observed quasars in the redshift bin. These data were drawn from *QuasarNet* - as collated in the Quasar Spectra Table and the Quasar Photometry Table per the schematic shown in Fig. 1. Each column corresponds to redshift bins ranging from $3 < z < 3.5$; $3.5 < z < 4.5$; $4.5 < z < 5.5$; $5.5 < z < 6.5$; and $z > 6.5$ respectively.

Acknowledgements

PN gratefully acknowledges the invitation to Google’s Science Festival SciFoo in 2018, where she first hatched this idea and thanks Sanjay Sarma and Brian Subirana at MIT for early discussions. She acknowledges Alphabet-X for technical support and computational resources for this project. PN and KST thank Rick Ebert at the Infra-Red Processing and Analysis Center (IPAC) at the California Institute of Technology for his help with accessing the NED database. KST thanks Frank Wang at Google for his help with the Google Cloud Platform. SK acknowledges use of the ARCHER UK National Super-computing Service (<http://www.archer.ac.uk>) for running the LEGACY simulation. BN acknowledges support from the Fermi National Accelerator Laboratory, managed and operated by Fermi Research Alliance, LLC under Contract No. DE-AC02-07CH11359 with the U.S. Department of Energy. The U.S. Government retains and the publisher, by accepting the article for publication, acknowledges that the U.S. Government retains a non-exclusive, paid-up, irrevocable, world-wide license to publish or reproduce the published form of this manuscript, or allow others to do so, for U.S. Government purposes. SS acknowledges the Aspen Center for Physics where parts of this work were done, which is supported by National Science Foundation grant PHY-1607611.

References

References

Abazajian, K.N., Adelman-McCarthy, J.K., Agüeros, M.A., et al., 2009. The Seventh Data Release of the Sloan Digital Sky Survey. *ApJS* 182, 543–558. doi:10.1088/0067-0049/182/2/543, [arXiv:0812.0649](https://arxiv.org/abs/0812.0649).

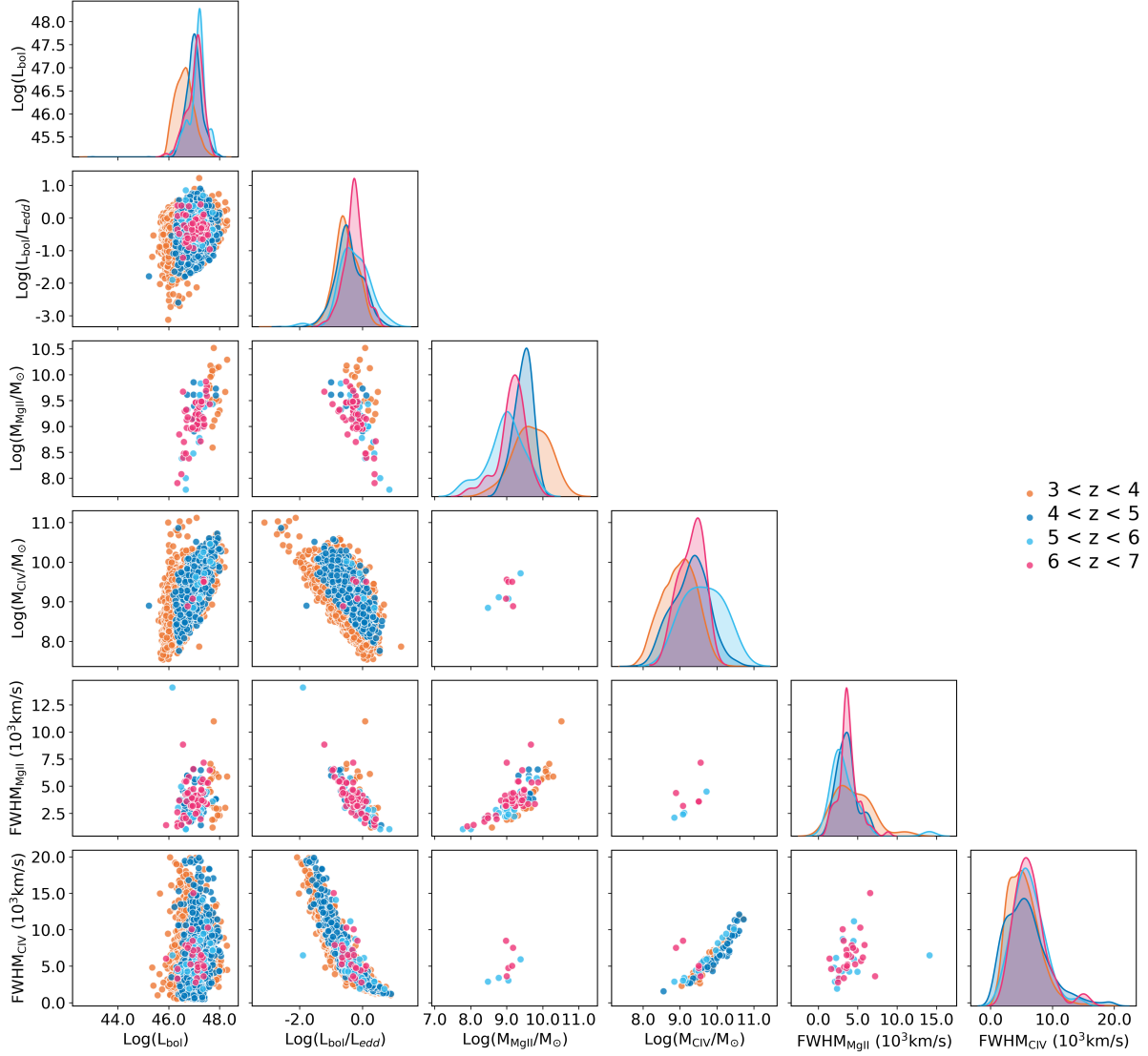


Figure 4: Preliminary exploration of correlations between properties of observed quasars in *QuasarNet* correlations between the bolometric luminosity; the Eddington ratio; BH mass determined from MgII line-widths; BH mass determined from CIV line-widths; the FWHM of MgII lines and the FWHM of CIV lines as compiled in the Quasar Spectra Table of *QuasarNet*. The data are color-coded according to redshift as follows: $3 < z < 4$ - orange; $4 < z < 5$ - blue; $5 < z < 6$ - cyan and $6 < z < 7$ - pink. Along the diagonal, we plot the kernel density estimations of the distributions for each of these parameters. The off-diagonal panels reveal the correlation between different pairs of parameters.

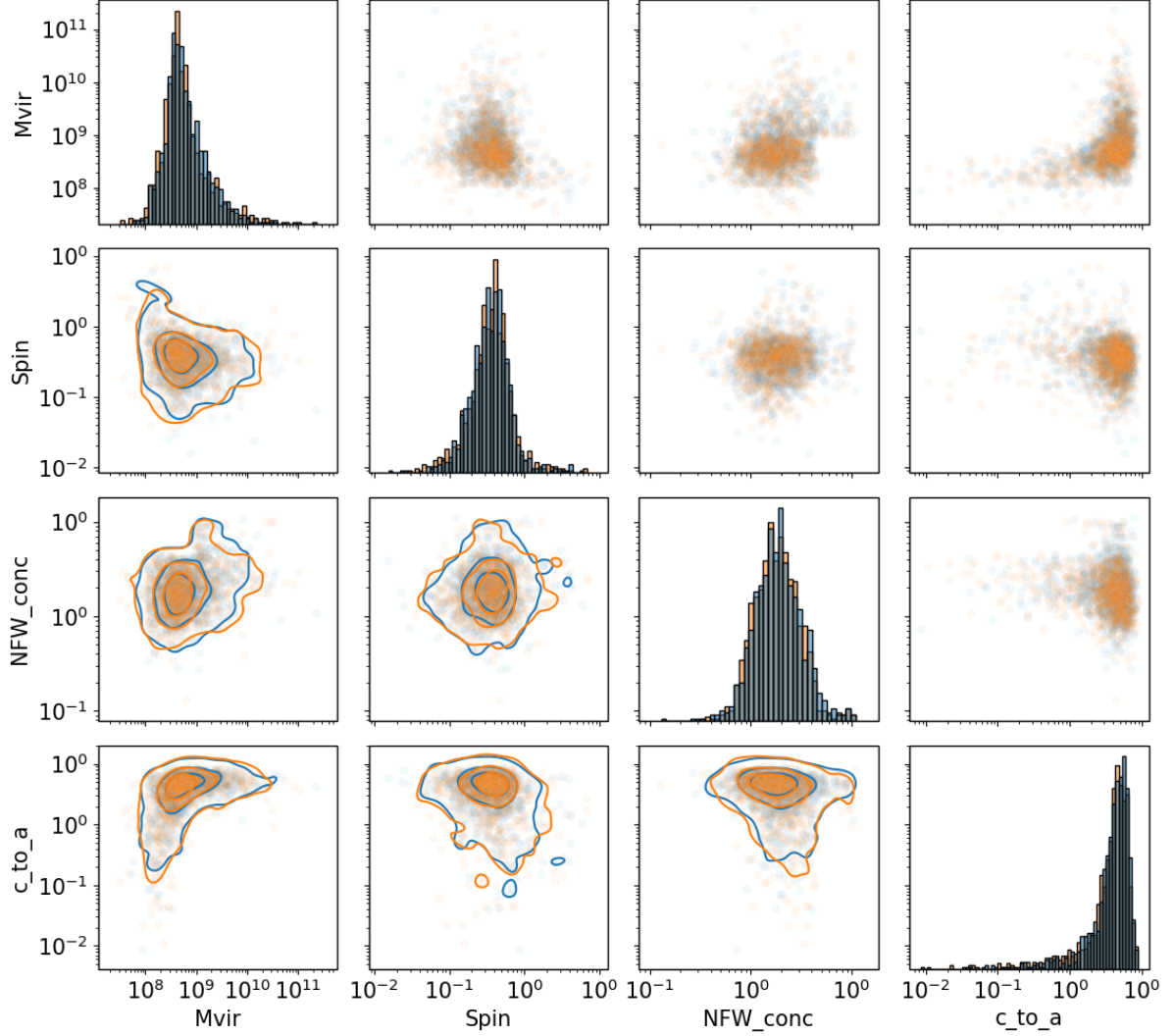


Figure 5: Derived underlying statistical properties of the dark matter halos at redshift $z = 3$ using ML techniques (normalizing flow). These derived prior distributions for halo properties are derived from the simulated halo catalogs. The distributions will be used to expand the LEGACY simulation volume to permit association studies of observed quasars from observational surveys with potential sites (parent dark matter halos). This is the first of the suite of tailored ML tools that we develop to fill in the key missing links to probe the black hole – host galaxy – parent dark matter halo connection. The distributions of "true" halo properties derived from the *QuasarNet* Halo Properties Table comprising the LEGACY simulation catalogs are colored in blue. Orange points are the ones generated by sampling with the trained normalizing flow model. While the model can be trained on the full table of available halo properties (81 available attributes) in *QuasarNet* here, we select the halo mass, halo spin, halo NFW concentration, and halo ellipticity as key characteristic properties to display. We note that the model captures the cross-correlation between the variables extremely well. This permits us to efficiently generate halos in larger simulation volumes that mimic observational surveys for our planned association studies that will facilitate downstream ML applications and tool development.

- Abdo, A.A., Ackermann, M., Ajello, M., et al., 2010. PKS 1502+106: A New and Distant Gamma-ray Blazar in Outburst Discovered by the Fermi Large Area Telescope. *ApJ* 710, 810–827. doi:10.1088/0004-637X/710/1/810, arXiv:0912.4029.
- Abolfathi, B., Aguado, D.S., Aguilar, G., et al., 2018. The Fourteenth Data Release of the Sloan Digital Sky Survey: First Spectroscopic Data from the Extended Baryon Oscillation Spectroscopic Survey and from the Second Phase of the Apache Point Observatory Galactic Evolution Experiment. *ApJS* 235, 42. doi:10.3847/1538-4365/aa9e8a, arXiv:1707.09322.
- Agarwal, B., Cullen, F., Khochfar, S., Ceverino, D., Klessen, R.S., 2019. Optimal neighbourhood to nurture giants: a fundamental link between star-forming galaxies and direct collapse black holes. *MNRAS* 488, 3268–3273. doi:10.1093/mnras/stz1347, arXiv:1808.09981.
- Agarwal, B., Dalla Vecchia, C., Johnson, J.L., Khochfar, S., Paardekoooper, J.P., 2014. The First Billion Years project: birthplaces of direct collapse black holes. *MNRAS* 443, 648–657. doi:10.1093/mnras/stu1112, arXiv:1403.5267.
- Alexander, D.M., Hickox, R.C., 2012. What drives the growth of black holes? *New A Rev.* 56, 93–121. doi:10.1016/j.newar.2011.11.003, arXiv:1112.1949.
- Alsing, J., Charnock, T., Feeney, S., Wandelt, B., 2019. Fast likelihood-free cosmology with neural density estimators and active learning. *Monthly Notices of the Royal Astronomical Society* URL: <http://dx.doi.org/10.1093/mnras/stz1960>, doi:10.1093/mnras/stz1960.
- Avni, Y., Bahcall, J.N., 1980. On the simultaneous analysis of several complete samples - The V/Vmax and Ve/Va variables, with applications to quasars. *ApJ* 235, 694–716. doi:10.1086/157673.
- Bañados, E., Venemans, B.P., Mazzucchelli, C., et al., 2018. An 800-million-solar-mass black hole in a significantly neutral Universe at a redshift of 7.5. *Nature* 553, 473–476. doi:10.1038/nature25180, arXiv:1712.01860.
- Barrow, K.S.S., Wise, J.H., Aykotalp, A., et al., 2018. First light - II. Emission line extinction, population III stars, and X-ray binaries. *MNRAS* 474, 2617–2634. doi:10.1093/mnras/stx2973, arXiv:1709.04473.
- Beckmann, R.S., Devriendt, J., Slyz, A., 2019. Zooming in on supermassive black holes: how resolving their gas cloud host renders their accretion episodic. *MNRAS* 483, 3488–3509. doi:10.1093/mnras/sty2890, arXiv:1810.01649.
- Beckmann, R.S., Slyz, A., Devriendt, J., 2018. Bondi or not Bondi: the impact of resolution on accretion and drag force modelling for supermassive black holes. *MNRAS* 478, 995–1016. doi:10.1093/mnras/sty931, arXiv:1803.03014.
- Behroozi, P.S., Wechsler, R.H., Wu, H.Y., 2013. The ROCKSTAR Phase-space Temporal Halo Finder and the Velocity Offsets of Cluster Cores. *ApJ* 762, 109. doi:10.1088/0004-637X/762/2/109, arXiv:1110.4372.
- Bentz, M.C., Manne-Nicholas, E., 2018. Black Hole-Galaxy Scaling Relationships for Active Galactic Nuclei with Reverberation Masses. *ApJ* 864, 146. doi:10.3847/1538-4357/aad808, arXiv:1808.01329.
- Bentz, M.C., Peterson, B.M., Netzer, H., Pogge, R.W., Vestergaard, M., 2009. The Radius-Luminosity Relationship for Active Galactic Nuclei: The Effect of Host-Galaxy Starlight on Luminosity Measurements. II. The Full Sample of Reverberation-Mapped AGNs. *ApJ* 697, 160–181. doi:10.1088/0004-637X/697/1/160, arXiv:0812.2283.
- Bernardini, M., Mayer, L., Reed, D., Feldmann, R., 2020. Predicting dark matter halo formation in N-body simulations with deep regression networks. *MNRAS* 496, 5116–5125. doi:10.1093/mnras/staa1911, arXiv:1912.04299.
- Beskin, V.S., Kuznetsova, I.V., 2000. On the Blandford-Znajek mechanism of the energy loss of a rotating black hole. *Nuovo Cimento B Serie* 115, 795. arXiv:astro-ph/0004021.
- Blandford, R.D., McKee, C.F., 1982. Reverberation mapping of the emission line regions of Seyfert galaxies and quasars. *ApJ* 255, 419–439. doi:10.1086/159843.
- Bower, R.G., Benson, A.J., Malbon, R., et al., 2006. Breaking the hierarchy of galaxy formation. *MNRAS* 370, 645–655. doi:10.1111/j.1365-2966.2006.10519.x, arXiv:astro-ph/0511338.
- Brown, M.J.I., Duncan, K.J., Landt, H., et al., 2019. The spectral energy distributions of active galactic nuclei. *MNRAS* 489, 3351–3367. doi:10.1093/mnras/stz2324, arXiv:1908.03720.
- Cadiou, C., Pontzen, A., Peiris, H.V., 2020. Angular momentum evolution can be predicted from cosmological initial conditions. *arXiv e-prints*, arXiv:2012.02201arXiv:2012.02201.
- Chen, C.T.J., Hickox, R.C., Alberts, S., et al., 2013. A Correlation between Star Formation Rate and Average Black Hole Accretion in Star-forming Galaxies. *ApJ* 773, 3. doi:10.1088/0004-637X/773/1/3, arXiv:1306.1227.
- Coatman, L., Hewett, P.C., Banerji, M., et al., 2017. Correcting C IV-based virial black hole masses. *MNRAS* 465, 2120–2142. doi:10.1093/mnras/stw2797, arXiv:1610.08977.
- Colpi, M., Holley-Bockelmann, K., Bogdanovic, T., et al., 2019. Astro2020 science white paper: The gravitational wave view of massive black holes. *arXiv e-prints*, arXiv:1903.06867arXiv:1903.06867.
- Cranmer, M.D., Galvez, R., Anderson, L., Spergel, D.N., Ho, S., 2019. Modeling the gaia color-magnitude diagram with bayesian neural flows to constrain distance estimates. arXiv:1908.08045.
- Dai, B., Seljak, U., 2020. Learning effective physical laws for generating cosmological hydrodynamics with Lagrangian Deep Learning. *arXiv e-prints*, arXiv:2010.02926arXiv:2010.02926.
- Davis, M., Efstathiou, G., Frenk, C.S., White, S.D.M., 1985. The evolution of large-scale structure in a universe dominated by cold dark matter. *ApJ* 292, 371–394. doi:10.1086/163168.
- De Rosa, G., Decarli, R., Walter, F., et al., 2011. Evidence for Non-evolving Fe II/Mg II Ratios in Rapidly Accreting $z \sim 6$ QSOs. *ApJ* 739, 56. doi:10.1088/0004-637X/739/2/56, arXiv:1106.5501.
- De Rosa, G., Venemans, B.P., Decarli, R., et al., 2014. Black Hole Mass Estimates and Emission-line Properties of a Sample of Redshift $z \gtrsim 6.5$ Quasars. *ApJ* 790, 145. doi:10.1088/0004-637X/790/2/145, arXiv:1311.3260.
- Debuhr, J., Quataert, E., Ma, C.P., 2011. The growth of massive black holes in galaxy merger simulations with feedback by radiation pressure. *MNRAS* 412, 1341–1360. doi:10.1111/j.1365-2966.2010.17992.x, arXiv:1006.3312.
- Di Matteo, T., Springel, V., Hernquist, L., 2005. Energy input from quasars regulates the growth and activity of black holes and their host galaxies. *Nature* 433, 604–607. doi:10.1038/nature03335, arXiv:astro-ph/0502199.
- Ding, X., Silverman, J., Treu, T., et al., 2020. The Mass Relations between Supermassive Black Holes and Their Host Galaxies at $1 \leq z \leq 2$ HST-WFC3. *ApJ* 888, 37. doi:10.3847/1538-4357/ab5b90, arXiv:1910.11875.
- Dinh, L., Sohl-Dickstein, J., Bengio, S., 2017. Density estimation using real nvp. arXiv:1605.08803.
- Dubois, Y., Devriendt, J., Slyz, A., Teyssier, R., 2012. Self-regulated growth of supermassive black holes by a dual jet-heating active galactic nucleus feedback mechanism: methods, tests and implications for cosmological simulations. *MNRAS* 420, 2662–2683. doi:10.1111/j.1365-2966.2011.20236.x, arXiv:1108.0110.
- Eilers, A.C., Hennawi, J.F., Davies, F.B., 2018. First Spectroscopic Study of a Young Quasar. *ApJ* 867, 30.

- doi:10.3847/1538-4357/aae081, arXiv:1806.05691.
- Event Horizon Telescope Collaboration, Akiyama, K., Alberdi, A., et al., 2019a. First M87 Event Horizon Telescope Results. I. The Shadow of the Supermassive Black Hole. *ApJ* 875, L1. doi:10.3847/2041-8213/ab0ec7, arXiv:1906.11238.
- Event Horizon Telescope Collaboration, Akiyama, K., Alberdi, A., et al., 2019b. First M87 Event Horizon Telescope Results. III. Data Processing and Calibration. *ApJ* 875, L3. doi:10.3847/2041-8213/ab0c57, arXiv:1906.11240.
- Ferrarese, L., Merritt, D., 2000. A Fundamental Relation between Supermassive Black Holes and Their Host Galaxies. *ApJ* 539, L9–L12. doi:10.1086/312838, arXiv:astro-ph/0006053.
- Gaibler, V., Khochfar, S., Krause, M., 2011. Asymmetries in extragalactic double radio sources: clues from 3D simulations of jet-disc interaction. *MNRAS* 411, 155–161. doi:10.1111/j.1365-2966.2010.17674.x, arXiv:1008.2757.
- Gammie, C.F., McKinney, J.C., Tóth, G., 2003. HARM: A Numerical Scheme for General Relativistic Magnetohydrodynamics. *ApJ* 589, 444–457. doi:10.1086/374594, arXiv:astro-ph/0301509.
- Gaspari, M., Tombesi, F., Cappi, M., 2020. Linking macro-, meso- and microscales in multiphase AGN feeding and feedback. *Nature Astronomy* 4, 10–13. doi:10.1038/s41550-019-0970-1, arXiv:2001.04985.
- Gebhardt, K., Bender, R., Bower, G., et al., 2000. A Relationship between Nuclear Black Hole Mass and Galaxy Velocity Dispersion. *ApJ* 539, L13–L16. doi:10.1086/312840, arXiv:astro-ph/0006289.
- Genzel, R., 2014. Massive Black Holes: Evidence, Demographics and Cosmic Evolution. arXiv e-prints, arXiv:1410.8717arXiv:1410.8717.
- Genzel, R., Eckart, A., Ott, T., Eisenhauer, F., 1997. On the nature of the dark mass in the centre of the Milky Way. *MNRAS* 291, 219–234. doi:10.1093/mnras/291.1.219.
- Ghez, A.M., Klein, B.L., Morris, M., Becklin, E.E., 1998. High Proper-Motion Stars in the Vicinity of Sagittarius A*: Evidence for a Supermassive Black Hole at the Center of Our Galaxy. *ApJ* 509, 678–686. doi:10.1086/306528, arXiv:astro-ph/9807210.
- Ghosh, A., Urry, C.M., Wang, Z., et al., 2020. Galaxy Morphology Network: A Convolutional Neural Network Used to Study Morphology and Quenching in $\sim 100,000$ SDSS and $\sim 20,000$ CANDELS Galaxies. *ApJ* 895, 112. doi:10.3847/1538-4357/ab8a47, arXiv:2006.14639.
- Giallongo, E., Grazian, A., Fiore, F., et al., 2015. Faint AGNs at $z > 4$ in the CANDELS GOODS-S field: looking for contributors to the reionization of the Universe. *A&A* 578, A83. doi:10.1051/0004-6361/201425334, arXiv:1502.02562.
- Glikman, E., Djorgovski, S.G., Stern, D., et al., 2011. The Faint End of the Quasar Luminosity Function at $z \sim 4$: Implications for Ionization of the Intergalactic Medium and Cosmic Downsizing. *ApJ* 728, L26. doi:10.1088/2041-8205/728/2/L26, arXiv:1101.0537.
- Grier, C.J., Pancoast, A., Barth, A.J., et al., 2017. The Structure of the Broad-line Region in Active Galactic Nuclei. II. Dynamical Modeling of Data From the AGN10 Reverberation Mapping Campaign. *ApJ* 849, 146. doi:10.3847/1538-4357/aa901b, arXiv:1705.02346.
- Gültekin, K., Richstone, D.O., Gebhardt, K., et al., 2009. The M - σ and M - L Relations in Galactic Bulges, and Determinations of Their Intrinsic Scatter. *ApJ* 698, 198–221. doi:10.1088/0004-637X/698/1/198, arXiv:0903.4897.
- Habouzit, M., Volonteri, M., Dubois, Y., 2017. Blossoms from black hole seeds: properties and early growth regulated by supernova feedback. *MNRAS* 468, 3935–3948. doi:10.1093/mnras/stx666, arXiv:1605.09394.
- Haehnelt, M.G., Natarajan, P., Rees, M.J., 1998. High-redshift galaxies, their active nuclei and central black holes. *MNRAS* 300, 817–827. doi:10.1046/j.1365-8711.1998.01951.x, arXiv:astro-ph/9712259.
- Hahn, O., Abel, T., 2011. Multi-scale initial conditions for cosmological simulations. *MNRAS* 415, 2101–2121. doi:10.1111/j.1365-2966.2011.18820.x, arXiv:1103.6031.
- Häring, N., Rix, H.W., 2004. On the Black Hole Mass-Bulge Mass Relation. *ApJ* 604, L89–L92. doi:10.1086/383567, arXiv:astro-ph/0402376.
- Harrison, C.M., Costa, T., Tadhunter, C.N., et al., 2018. AGN outflows and feedback twenty years on. *Nature Astronomy* 2, 198–205. doi:10.1038/s41550-018-0403-6, arXiv:1802.10306.
- Hasinger, G., 2008. Absorption properties and evolution of active galactic nuclei. *A&A* 490, 905–922. doi:10.1051/0004-6361/200809839, arXiv:0808.0260.
- Hawley, J.F., Beckwith, K., Krolik, J.H., 2007. General relativistic MHD simulations of black hole accretion disks and jets. *Ap&SS* 311, 117–125. doi:10.1007/s10509-007-9559-8.
- He, S., Li, Y., Feng, Y., et al., 2019. Learning to predict the cosmological structure formation. *Proceedings of the National Academy of Sciences* 116, 13825–13832. URL: <https://www.pnas.org/content/116/28/13825>, doi:10.1073/pnas.1821458116, arXiv:https://www.pnas.org/content/116/28/13825.full.pdf.
- Heckman, T.M., Best, P.N., 2014. The Coevolution of Galaxies and Supermassive Black Holes: Insights from Surveys of the Contemporary Universe. *ARA&A* 52, 589–660. doi:10.1146/annurev-astro-081913-035722, arXiv:1403.4620.
- Hinshaw, G., Larson, D., Komatsu, E., et al., 2013. Nine-year Wilkinson Microwave Anisotropy Probe (WMAP) Observations: Cosmological Parameter Results. *ApJS* 208, 19. doi:10.1088/0067-0049/208/2/19, arXiv:1212.5226.
- Hirschmann, M., Khochfar, S., Burkert, A., et al., 2010. On the evolution of the intrinsic scatter in black hole versus galaxy mass relations. *MNRAS* 407, 1016–1032. doi:10.1111/j.1365-2966.2010.17006.x, arXiv:1005.2100.
- Hortúa, H.J., Volpi, R., Marinelli, D., Malagò, L., 2020. Parameter estimation for the cosmic microwave background with Bayesian neural networks. *Phys. Rev. D* 102, 103509. doi:10.1103/PhysRevD.102.103509, arXiv:1911.08508.
- Hortúa, H.J., Malagò, L., Volpi, R., 2020. Constraining the reionization history using bayesian normalizing flows. *Machine Learning: Science and Technology* 1, 035014. URL: <http://dx.doi.org/10.1088/2632-2153/aba6f1>, doi:10.1088/2632-2153/aba6f1.
- Jahnke, K., Macciò, A.V., 2011. The Non-causal Origin of the Black-hole-galaxy Scaling Relations. *ApJ* 734, 92. doi:10.1088/0004-637X/734/2/92, arXiv:1006.0482.
- Jiang, L., Fan, X., Vestergaard, M., et al., 2007. Gemini Near-Infrared Spectroscopy of Luminous $z \sim 6$ Quasars: Chemical Abundances, Black Hole Masses, and Mg II Absorption. *AJ* 134, 1150. doi:10.1086/520811, arXiv:0707.1663.
- Jiang, L., McGreer, I.D., Fan, X., et al., 2016. The Final SDSS High-redshift Quasar Sample of 52 Quasars at $z > 5.7$. *ApJ* 833, 222. doi:10.3847/1538-4357/833/2/222, arXiv:1610.05369.
- Jurić, M., Kantor, J., Lim, K.T., et al., 2017. The LSST Data Management System, in: Lorente, N.P.F., Shortridge, K., Wayth, R. (Eds.), *Astronomical Data Analysis Software and Systems XXV*, p. 279. arXiv:1512.07914.
- Kamdar, H.M., Turk, M.J., Brunner, R.J., 2016. Machine learning and cosmological simulations - II. Hydrodynamical

- simulations. *MNRAS* 457, 1162–1179. doi:10.1093/mnras/stv2981, arXiv:1510.07659.
- Kashikawa, N., Ishizaki, Y., Willott, C.J., et al., 2015. The Subaru High- z Quasar Survey: Discovery of Faint $z \sim 6$ Quasars. *ApJ* 798, 28. doi:10.1088/0004-637X/798/1/28, arXiv:1410.7401.
- Kaspi, S., Maoz, D., Netzer, H., et al., 2005. The Relationship between Luminosity and Broad-Line Region Size in Active Galactic Nuclei. *ApJ* 629, 61–71. doi:10.1086/431275, arXiv:astro-ph/0504484.
- Kaspi, S., Smith, P.S., Netzer, H., et al., 2000. Reverberation Measurements for 17 Quasars and the Size-Mass-Luminosity Relations in Active Galactic Nuclei. *ApJ* 533, 631–649. doi:10.1086/308704, arXiv:astro-ph/9911476.
- Katz, M.L., Kelley, L.Z., Dosopoulou, F., et al., 2020. Probing massive black hole binary populations with LISA. *MNRAS* 491, 2301–2317. doi:10.1093/mnras/stz3102, arXiv:1908.05779.
- Kelley, L.Z., Blecha, L., Hernquist, L., Sesana, A., Taylor, S.R., 2018. Single sources in the low-frequency gravitational wave sky: properties and time to detection by pulsar timing arrays. *MNRAS* 477, 964–976. doi:10.1093/mnras/sty689, arXiv:1711.00075.
- Kelly, B.C., Shen, Y., 2013. The Demographics of Broad-line Quasars in the Mass-Luminosity Plane. II. Black Hole Mass and Eddington Ratio Functions. *ApJ* 764, 45. doi:10.1088/0004-637X/764/1/45, arXiv:1209.0477.
- Kelly, B.C., Vestergaard, M., Fan, X., et al., 2010. CONSTRAINTS ON BLACK HOLE GROWTH, QUASAR LIFETIMES, AND EDDINGTON RATIO DISTRIBUTIONS FROM THE SDSS BROAD-LINE QUASAR BLACK HOLE MASS FUNCTION. *The Astrophysical Journal* 719, 1315–1334. URL: <https://doi.org/10.1088/0004-637x/719/2/1315>, doi:10.1088/0004-637x/719/2/1315.
- Kingma, D.P., Salimans, T., Jozefowicz, R., et al., 2017. Improving variational inference with inverse autoregressive flow. arXiv:1606.04934.
- Klypin, A., Prada, F., 2019. Effects of long-wavelength fluctuations in large galaxy surveys. *MNRAS* 489, 1684–1696. doi:10.1093/mnras/stz2194, arXiv:1809.03637.
- Komissarov, S., 2005. Simulations of Black Hole Magnetospheres, in: KITP Conference: Physics of Astrophysical Outflows and Accretion Disks, p. 15.
- Komissarov, S.S., 2001. Direct numerical simulations of the Blandford-Znajek effect. *MNRAS* 326, L41–L44. doi:10.1046/j.1365-8711.2001.04863.x.
- Kormendy, J., Ho, L.C., 2013. Coevolution (Or Not) of Supermassive Black Holes and Host Galaxies. *ARA&A* 51, 511–653. doi:10.1146/annurev-astro-082708-101811, arXiv:1304.7762.
- Kozłowski, S., 2017. Virial Black Hole Mass Estimates for 280,000 AGNs from the SDSS Broadband Photometry and Single-epoch Spectra. *ApJS* 228, 9. doi:10.3847/1538-4365/228/1/9, arXiv:1609.09489.
- Kulkarni, G., Worseck, G., Hennawi, J.F., 2019. Evolution of the AGN UV luminosity function from redshift 7.5. *MNRAS* 488, 1035–1065. doi:10.1093/mnras/stz1493, arXiv:1807.09774.
- Kurk, J.D., Walter, F., Fan, X., et al., 2007. Black Hole Masses and Enrichment of $z \sim 6$ SDSS Quasars. *ApJ* 669, 32–44. doi:10.1086/521596, arXiv:0707.1662.
- Latif, M.A., Khochfar, S., 2020. Inception of a first quasar at cosmic dawn. *MNRAS* 497, 3761–3769. doi:10.1093/mnras/staa2218, arXiv:2005.10436.
- Liska, M., Hesp, C., Tchekhovskoy, A., et al., 2018. Formation of precessing jets by tilted black hole discs in 3D general relativistic MHD simulations. *MNRAS* 474, L81–L85. doi:10.1093/mnras/1/slx174, arXiv:1707.06619.
- Lodato, G., Natarajan, P., 2006. Supermassive black hole formation during the assembly of pre-galactic discs. *MNRAS* 371, 1813–1823. doi:10.1111/j.1365-2966.2006.10801.x, arXiv:astro-ph/0606159.
- Lodato, G., Natarajan, P., 2007. The mass function of high-redshift seed black holes. *MNRAS* 377, L64–L68. doi:10.1111/j.1745-3933.2007.00304.x, arXiv:astro-ph/0702340.
- LSST Science Collaboration, Abell, P.A., Allison, J., et al., 2009. LSST Science Book, Version 2.0. arXiv e-prints , arXiv:0912.0201arXiv:0912.0201.
- Lucie-Smith, L., Peiris, H.V., Pontzen, A., Nord, B., Thiyaalingam, J., 2020. Deep learning insights into cosmological structure formation. arXiv e-prints , arXiv:2011.10577arXiv:2011.10577.
- Magorrian, J., Tremaine, S., Richstone, D., et al., 1998. The Demography of Massive Dark Objects in Galaxy Centers. *AJ* 115, 2285–2305. doi:10.1086/300353, arXiv:astro-ph/9708072.
- Marziani, P., del Olmo, A., Martínez-Carballo, M.A., et al., 2019. Black hole mass estimates in quasars. A comparative analysis of high- and low-ionization lines. *A&A* 627, A88. doi:10.1051/0004-6361/201935265, arXiv:1905.00617.
- Matsuoka, Y., Onoue, M., Kashikawa, N., et al., 2019. Discovery of the First Low-luminosity Quasar at $z \gtrsim 7$. *ApJ* 872, L2. doi:10.3847/2041-8213/ab0216, arXiv:1901.10487.
- Mazzucchelli, C., Bañados, E., Venemans, B.P., et al., 2017. Physical Properties of 15 Quasars at $z \gtrsim 6.5$. *ApJ* 849, 91. doi:10.3847/1538-4357/aa9185, arXiv:1710.01251.
- McConnell, N.J., Ma, C.P., 2013. Revisiting the Scaling Relations of Black Hole Masses and Host Galaxy Properties. *ApJ* 764, 184. doi:10.1088/0004-637X/764/2/184, arXiv:1211.2816.
- McGreer, I.D., Jiang, L., Fan, X., et al., 2013. The $z = 5$ Quasar Luminosity Function from SDSS Stripe 82. *ApJ* 768, 105. doi:10.1088/0004-637X/768/2/105, arXiv:1212.4493.
- McKinney, J.C., 2005. Total and Jet Blandford-Znajek Power in the Presence of an Accretion Disk. *ApJ* 630, L5–L8. doi:10.1086/468184, arXiv:astro-ph/0506367.
- Miyoshi, M., Moran, J., Herrnstein, J., et al., 1995. Evidence for a black hole from high rotation velocities in a sub-parsec region of NGC4258. *Nature* 373, 127–129. doi:10.1038/373127a0.
- Mortlock, D.J., Warren, S.J., Venemans, B.P., et al., 2011. A luminous quasar at a redshift of $z = 7.085$. *Nature* 474, 616–619. doi:10.1038/nature10159, arXiv:1106.6088.
- Moster, B.P., Naab, T., Lindström, M., O’Leary, J.A., 2020. GalaxyNet: Connecting galaxies and dark matter haloes with deep neural networks and reinforcement learning in large volumes. arXiv e-prints , arXiv:2005.12276arXiv:2005.12276.
- Nandra, K., O’Neill, P.M., George, I.M., Reeves, J.N., Turner, T.J., 2006. An XMM-Newton survey of broad iron lines in AGN. *Astronomische Nachrichten* 327, 1039. doi:10.1002/asna.200610641, arXiv:astro-ph/0610585.
- Natarajan, P., 2014. Seeds to monsters: tracing the growth of black holes in the universe. *General Relativity and Gravitation* 46, 1702. doi:10.1007/s10714-014-1702-6.
- Natarajan, P., Pacucci, F., Ferrara, A., et al., 2017. Unveiling the first black holes With JWST: multi-wavelength spectral predictions. *The Astrophysical Journal* 838, 117. URL: <https://doi.org/10.3847/2F1538-4357/2Faa6330>,

- doi:10.3847/1538-4357/aa6330.
- Natarajan, P., Ricarte, A., Baldassare, V., et al., 2019. Disentangling nature from nurture: tracing the origin of seed black holes. *BAAS* 51, 73. [arXiv:1904.09326](#).
- Natarajan, P., Treister, E., 2009. Is there an upper limit to black hole masses? *MNRAS* 393, 838–845. doi:10.1111/j.1365-2966.2008.13864.x, [arXiv:0808.2813](#).
- Nelson, D., Pillepich, A., Genel, S., et al., 2015. The illustris simulation: Public data release. *Astronomy and Computing* 13, 12–37. doi:10.1016/j.ascom.2015.09.003, [arXiv:1504.00362](#).
- Netzer, H., 2015. Revisiting the Unified Model of Active Galactic Nuclei. *ARA&A* 53, 365–408. doi:10.1146/annurev-astro-082214-122302, [arXiv:1505.00811](#).
- Nord, B., Connolly, A.J., Kinney, J., et al., 2019. Algorithms and Statistical Models for Scientific Discovery in the Petabyte Era, in: *Bulletin of the American Astronomical Society*, p. 224. [arXiv:1911.02479](#).
- Ntampaka, M., Avestruz, C., Boada, S., et al., 2019. The Role of Machine Learning in the Next Decade of Cosmology. *BAAS* 51, 14. [arXiv:1902.10159](#).
- Ntampaka, M., Eisenstein, D.J., Yuan, S., Garrison, L.H., 2020. A Hybrid Deep Learning Approach to Cosmological Constraints from Galaxy Redshift Surveys. *ApJ* 889, 151. doi:10.3847/1538-4357/ab5f5e, [arXiv:1909.10527](#).
- Pacucci, F., Ferrara, A., Grazian, A., et al., 2016. First identification of direct collapse black hole candidates in the early Universe in CANDELS/GOODS-S. *MNRAS* 459, 1432–1439. doi:10.1093/mnras/stw725, [arXiv:1603.08522](#).
- Papamakarios, G., Pavlakou, T., Murray, I., 2018. Masked autoregressive flow for density estimation. [arXiv:1705.07057](#).
- Peng, C.Y., 2007. How Mergers May Affect the Mass Scaling Relation between Gravitationally Bound Systems. *ApJ* 671, 1098–1107. doi:10.1086/522774, [arXiv:0704.1860](#).
- Peterson, B.M., 1993. Reverberation Mapping of Active Galactic Nuclei. *PASP* 105, 247. doi:10.1086/133140.
- Peterson, B.M., 2014. Measuring the Masses of Supermassive Black Holes. *Space Sci. Rev.* 183, 253–275. doi:10.1007/s11214-013-9987-4.
- Peterson, B.M., Ferrarese, L., Gilbert, K.M., et al., 2004. Central Masses and Broad-Line Region Sizes of Active Galactic Nuclei. II. A Homogeneous Analysis of a Large Reverberation-Mapping Database. *ApJ* 613, 682–699. doi:10.1086/423269, [arXiv:astro-ph/0407299](#).
- Phipps, F., Khochfar, S., Varri, A.L., Dalla Vecchia, C., 2020. The First Billion Years project: Finding infant globular clusters at $z = 6$. *A&A* 641, A132. doi:10.1051/0004-6361/202037884, [arXiv:1910.09924](#).
- Reynolds, C.S., 2020. Observational Constraints on Black Hole Spin. *arXiv e-prints*, [arXiv:2011.08948](#) [arXiv:2011.08948](#).
- Rezende, D.J., Mohamed, S., 2016. Variational inference with normalizing flows. [arXiv:1505.05770](#).
- Ricarte, A., Natarajan, P., 2018a. Exploring SMBH assembly with semi-analytic modelling. *MNRAS* 474, 1995–2011. doi:10.1093/mnras/stx2851, [arXiv:1710.11532](#).
- Ricarte, A., Natarajan, P., 2018b. The observational signatures of supermassive black hole seeds. *MNRAS* 481, 3278–3292. doi:10.1093/mnras/sty2448, [arXiv:1809.01177](#).
- Ricarte, A., Tremmel, M., Natarajan, P., Quinn, T., 2019. Tracing black hole and galaxy co-evolution in the ROMULUS simulations. *MNRAS* 489, 802–819. doi:10.1093/mnras/stz2161, [arXiv:1904.10116](#).
- Richards, G.T., Fan, X., Newberg, H.J., et al., 2002. Spectroscopic Target Selection in the Sloan Digital Sky Survey: The Quasar Sample. *AJ* 123, 2945–2975. doi:10.1086/340187, [arXiv:astro-ph/0202251](#).
- Robertson, B., Bullock, J.S., Cox, T.J., et al., 2006. A Merger-driven Scenario for Cosmological Disk Galaxy Formation. *ApJ* 645, 986–1000. doi:10.1086/504412, [arXiv:astro-ph/0503369](#).
- Ross, N.P., McGreer, I.D., White, M., et al., 2013. The SDSS-III Baryon Oscillation Spectroscopic Survey: The Quasar Luminosity Function from Data Release Nine. *ApJ* 773, 14. doi:10.1088/0004-637X/773/1/14, [arXiv:1210.6389](#).
- Salvato, M., Ilbert, O., Hoyle, B., 2019. The many flavours of photometric redshifts. *Nature Astronomy* 3, 212–222. doi:10.1038/s41550-018-0478-0, [arXiv:1805.12574](#).
- Schawinski, K., Zhang, C., Zhang, H., Fowler, L., Santhanam, G.K., 2017. Generative adversarial networks recover features in astrophysical images of galaxies beyond the deconvolution limit. *MNRAS* 467, L110–L114. doi:10.1093/mnrasl/slx008, [arXiv:1702.00403](#).
- Schaye, J., Crain, R.A., Bower, R.G., et al., 2015. The EAGLE project: simulating the evolution and assembly of galaxies and their environments. *MNRAS* 446, 521–554. doi:10.1093/mnras/stu2058, [arXiv:1407.7040](#).
- Schneider, D.P., Richards, G.T., Hall, P.B., et al., 2010. The Sloan Digital Sky Survey Quasar Catalog. V. Seventh Data Release. *AJ* 139, 2360. doi:10.1088/0004-6256/139/6/2360, [arXiv:1004.1167](#).
- Sexton, R.O., Canalizo, G., Hiner, K.D., et al., 2019. Stronger Constraints on the Evolution of the M_{BH} Relation up to $z = 0.6$. *ApJ* 878, 101. doi:10.3847/1538-4357/ab21d5, [arXiv:1905.05780](#).
- Shao, Y., Wang, R., Jones, G.C., et al., 2017. Gas Dynamics of a Luminous $z = 6.13$ Quasar ULAS J1319+0950 Revealed by ALMA High-resolution Observations. *ApJ* 845, 138. doi:10.3847/1538-4357/aa826c, [arXiv:1707.03078](#).
- Shen, Y., 2013. The mass of quasars. *Bulletin of the Astronomical Society of India* 41, 61–115. [arXiv:1302.2643](#).
- Shen, Y., Hall, P.B., Horne, K., et al., 2019a. The Sloan Digital Sky Survey Reverberation Mapping Project: Sample Characterization. *ApJS* 241, 34. doi:10.3847/1538-4365/ab074f, [arXiv:1810.01447](#).
- Shen, Y., Liu, X., 2012. Comparing Single-epoch Virial Black Hole Mass Estimators for Luminous Quasars. *ApJ* 753, 125. doi:10.1088/0004-637X/753/2/125, [arXiv:1203.0601](#).
- Shen, Y., Liu, X., 2012. COMPARING SINGLE-EPOCH VIRIAL BLACK HOLE MASS ESTIMATORS FOR LUMINOUS QUASARS. *The Astrophysical Journal* 753, 125. URL: <https://doi.org/10.1088/0004-637X/753/2/125>, doi:10.1088/0004-637X/753/2/125.
- Shen, Y., Richards, G.T., Strauss, M.A., et al., 2011. A Catalog of Quasar Properties from Sloan Digital Sky Survey Data Release 7. *ApJS* 194, 45. doi:10.1088/0067-0049/194/2/45, [arXiv:1006.5178](#).
- Shen, Y., Wu, J., Jiang, L., et al., 2019b. Gemini GNIRS Near-infrared Spectroscopy of 50 Quasars at $z \gtrsim 5.7$. *ApJ* 873, 35. doi:10.3847/1538-4357/ab03d9, [arXiv:1809.05584](#).
- Sijacki, D., Springel, V., Di Matteo, T., Hernquist, L., 2007. A unified model for AGN feedback in cosmological simulations of structure formation. *MNRAS* 380, 877–900. doi:10.1111/j.1365-2966.2007.12153.x, [arXiv:0705.2238](#).
- Sijacki, D., Vogelsberger, M., Genel, S., et al., 2015. The Illustris simulation: the evolving population of black holes across cosmic time. *MNRAS* 452, 575–596. doi:10.1093/mnras/stv1340, [arXiv:1408.6842](#).
- Small, T.A., Blandford, R.D., 1992. Quasar evolution and the growth of black holes. *MNRAS* 259, 725–737.

- doi:10.1093/mnras/259.4.725.
- Springel, V., Di Matteo, T., Hernquist, L., 2005a. Modelling feedback from stars and black holes in galaxy mergers. MNRAS 361, 776–794. doi:10.1111/j.1365-2966.2005.09238.x, arXiv:astro-ph/0411108.
- Springel, V., Di Matteo, T., Hernquist, L., 2005b. Modelling feedback from stars and black holes in galaxy mergers. MNRAS 361, 776–794. doi:10.1111/j.1365-2966.2005.09238.x, arXiv:astro-ph/0411108.
- Springel, V., Frenk, C.S., White, S.D.M., 2006. The large-scale structure of the Universe. Nature 440, 1137–1144. doi:10.1038/nature04805, arXiv:astro-ph/0604561.
- Springel, V., White, S.D.M., Tormen, G., Kauffmann, G., 2001. Populating a cluster of galaxies - I. Results at $[z=0]$. MNRAS 328, 726–750. doi:10.1046/j.1365-8711.2001.04912.x, arXiv:astro-ph/0012055.
- Steidel, C.C., Adelberger, K.L., Giavalisco, M., Dickinson, M., Pettini, M., 1999. Lyman-break galaxies at $z \sim 4$. `\documentclass{aastex}` `\usepackage{amsmath}` `\usepackage{amssymb}` `\usepackage{bm}` `\usepackage{mathrsfs}` `\usepackage{pifont}` `\usepackage{stmaryrd}` `\usepackage{textcomp}` `\usepackage{portland,xspace}` `\usepackage{amsmath,amsxtra}` `\usepackage[OT2,OT1]{fontenc}` `\newcommand{\cyr}{\renewcommand{\rmdefault}{wncyr} \renewcommand{\sfdefault}{wncys} \renewcommand{\encodingdefault}{OT2} \normalfont \selectfont \DeclareTextFontCommand{\textcyr}{\cyr} \pagestyle{empty} \DeclareMathSizes{10}{9}{7}{6} \begin{document} \landscape $z_{\rm trsim} 4$ \end{document}` and the evolution of the ultraviolet luminosity density at high redshift. The Astrophysical Journal 519, 1–17. URL: <https://doi.org/10.1086/307363>, doi:10.1086/307363.
- Storchi-Bergmann, T., Schnorr-Müller, A., 2019. Observational constraints on the feeding of supermassive black holes. Nature Astronomy 3, 48–61. doi:10.1038/s41550-018-0611-0, arXiv:1904.03338.
- Taylor, S., Burke-Spolaor, S., Baker, P.T., et al., 2019. Supermassive Black-hole Demographics & Environments With Pulsar Timing Arrays. BAAS 51, 336. arXiv:1903.08183.
- Tchekhovskoy, A., Narayan, R., McKinney, J.C., 2010. Black Hole Spin and The Radio Loud/Quiet Dichotomy of Active Galactic Nuclei. ApJ 711, 50–63. doi:10.1088/0004-637X/711/1/50, arXiv:0911.2228.
- Tchekhovskoy, A., Narayan, R., McKinney, J.C., 2011. Efficient generation of jets from magnetically arrested accretion on a rapidly spinning black hole. MNRAS 418, L79–L83. doi:10.1111/j.1745-3933.2011.01147.x, arXiv:1108.0412.
- Trakhtenbrot, B., Netzer, H., 2012. Black hole growth to $z = 2$ - I. Improved virial methods for measuring M_{BH} and L_{Edd} . MNRAS 427, 3081–3102. doi:10.1111/j.1365-2966.2012.22056.x, arXiv:1209.1096.
- Trakhtenbrot, B., Netzer, H., Lira, P., Shemmer, O., 2011. Black Hole Mass and Growth Rate at $z \sim 4.8$: A Short Episode of Fast Growth Followed by Short Duty Cycle Activity. ApJ 730, 7. doi:10.1088/0004-637X/730/1/7, arXiv:1012.1871.
- Treister, E., Schawinski, K., Volonteri, M., Natarajan, P., Gawiser, E., 2011. Black hole growth in the early Universe is self-regulated and largely hidden from view. Nature 474, 356–358. doi:10.1038/nature10103, arXiv:1106.3079.
- Tremaine, S., Gebhardt, K., Bender, R., et al., 2002. The Slope of the Black Hole Mass versus Velocity Dispersion Correlation. ApJ 574, 740–753. doi:10.1086/341002, arXiv:astro-ph/0203468.
- Tremaine, S., Richstone, D.O., Byun, Y.I., et al., 1994. A Family of Models for Spherical Stellar Systems. AJ 107, 634. doi:10.1086/116883, arXiv:astro-ph/9309044.
- Urry, C.M., Padovani, P., 1995. Unified Schemes for Radio-Loud Active Galactic Nuclei. PASP 107, 803. doi:10.1086/133630, arXiv:astro-ph/9506063.
- Vanden Berk, D.E., Richards, G.T., Bauer, A., et al., 2001. Composite Quasar Spectra from the Sloan Digital Sky Survey. AJ 122, 549–564. doi:10.1086/321167, arXiv:astro-ph/0105231.
- Venemans, B.P., Bañados, E., Decarli, R., et al., 2015. The Identification of Z-dropouts in Pan-STARRS1: Three Quasars at $6.5 < z < 6.7$. ApJ 801, L11. doi:10.1088/2041-8205/801/1/L11, arXiv:1502.01927.
- Vestergaard, M., 2019. Black hole masses in active galactic nuclei. Nature Astronomy 3, 11–12. doi:10.1038/s41550-018-0670-2.
- Vestergaard, M., Osmer, P.S., 2009. Mass Functions of the Active Black Holes in Distant Quasars from the Large Bright Quasar Survey, the Bright Quasar Survey, and the Color-selected Sample of the SDSS Fall Equatorial Stripe. ApJ 699, 800–816. doi:10.1088/0004-637X/699/1/800, arXiv:0904.3348.
- Vestergaard, M., Peterson, B.M., 2006. Determining Central Black Hole Masses in Distant Active Galaxies and Quasars. II. Improved Optical and UV Scaling Relationships. ApJ 641, 689–709. doi:10.1086/500572, arXiv:astro-ph/0601303.
- Vogelsberger, M., Genel, S., Springel, V., et al., 2014. Introducing the Illustris Project: simulating the coevolution of dark and visible matter in the Universe. MNRAS 444, 1518–1547. doi:10.1093/mnras/stu1536, arXiv:1405.2921.
- Volonteri, M., 2012. The Formation and Evolution of Massive Black Holes. Science 337, 544. doi:10.1126/science.1220843, arXiv:1208.1106.
- Weinberger, R., Springel, V., Pakmor, R., et al., 2018. Supermassive black holes and their feedback effects in the IllustrisTNG simulation. MNRAS 479, 4056–4072. doi:10.1093/mnras/sty1733, arXiv:1710.04659.
- Willott, C.J., Albert, L., Arzoumanian, D., et al., 2010a. Eddington-limited Accretion and the Black Hole Mass Function at Redshift 6. AJ 140, 546–560. doi:10.1088/0004-6256/140/2/546, arXiv:1006.1342.
- Willott, C.J., Delorme, P., Reylé, C., et al., 2010b. The Canada-France High- z Quasar Survey: Nine New Quasars and the Luminosity Function at Redshift 6. AJ 139, 906–918. doi:10.1088/0004-6256/139/3/906, arXiv:0912.0281.
- Wise, J.H., Regan, J.A., O’Shea, B.W., et al., 2019. Formation of massive black holes in rapidly growing pre-galactic gas clouds. Nature 566, 85–88. doi:10.1038/s41586-019-0873-4, arXiv:1901.07563.
- Woo, J.H., Yoon, Y., Park, S., Park, D., Kim, S.C., 2015. The Black Hole Mass-Stellar Velocity Dispersion Relation of Narrow-line Seyfert 1 Galaxies. ApJ 801, 38. doi:10.1088/0004-637X/801/1/38, arXiv:1412.7225.
- Woods, T.E., Agarwal, B., Bromm, V., et al., 2019. Titans of the early Universe: The Prato statement on the origin of the first supermassive black holes. PASA 36, e027. doi:10.1017/pasa.2019.14, arXiv:1810.12310.
- Yang, J., Wang, F., Wu, X.B., et al., 2016. A Survey of Luminous High-redshift Quasars with SDSS and WISE. II. the Bright End of the Quasar Luminosity Function at $z \approx 5$. ApJ 829, 33. doi:10.3847/0004-637X/829/1/33, arXiv:1607.04415.
- Yao-Yu Lin, J., Pandya, S., Pratap, D., Liu, X., Carrasco Kind, M., 2020. AGNet: Weighing Black Holes with Machine Learning. arXiv e-prints , arXiv:2011.15095, arXiv:2011.15095.
- Znajek, R.L., 1977. Black hole electrodynamics and the Carter tetrad. MNRAS 179, 457–472. doi:10.1093/mnras/179.3.457.

SUPPLEMENTARY MATERIALS

In this section, we outline the current understanding of the connection between galaxies and their central SMBHs to provide the context for our specific project. This discussion includes a brief taxonomy of accreting massive BHs, a summary of models and the observational data that supports the current paradigm. We discuss the essential theoretical and observational characteristics of accreting SMBHs, the presently known correlations between galaxy properties and BH mass, and the population statistics relevant for the data-driven investigations explored in this work.

4.6. Active Galactic Nuclei (AGN)

Less than a parsec across, the nucleus of a typical galaxy appears to harbor a central SMBH Genzel (2014). A galactic nucleus is considered active when a hot and geometrically thin disk of accreting gas surrounds a central SMBH. While incomplete, there exist descriptions of unified models for active galactic nuclei (AGN) that describe their dynamics and account for their properties across a large range of physical scales around the growing BH (for example the proposal to unify all Radio-Loud AGN is presented in Urry and Padovani (1995)). Per the unified schemes, on small scales, ultraviolet radiation that is emitted by the accretion disk illuminates small, closely orbiting gas clouds and on larger scales, the disk is inferred to be surrounded by a puffed-up toroidal region that consists of dusty molecular gas. Accretion activity is believed to be episodic, lasting $\lesssim 10^8$ years, during the life cycle of a galaxy, during which it can produce a tremendous amount of energy, often outshining the entire stellar content of the galaxy by several orders of magnitude. Integrating the various physical scales and the coupling of astrophysical processes therein has been the aspiration of modeling efforts to date. We describe the observational signatures of black hole activity that arise on full the range of scales across wavelengths that are now integrated in a convenient form in *QuasarNet*.

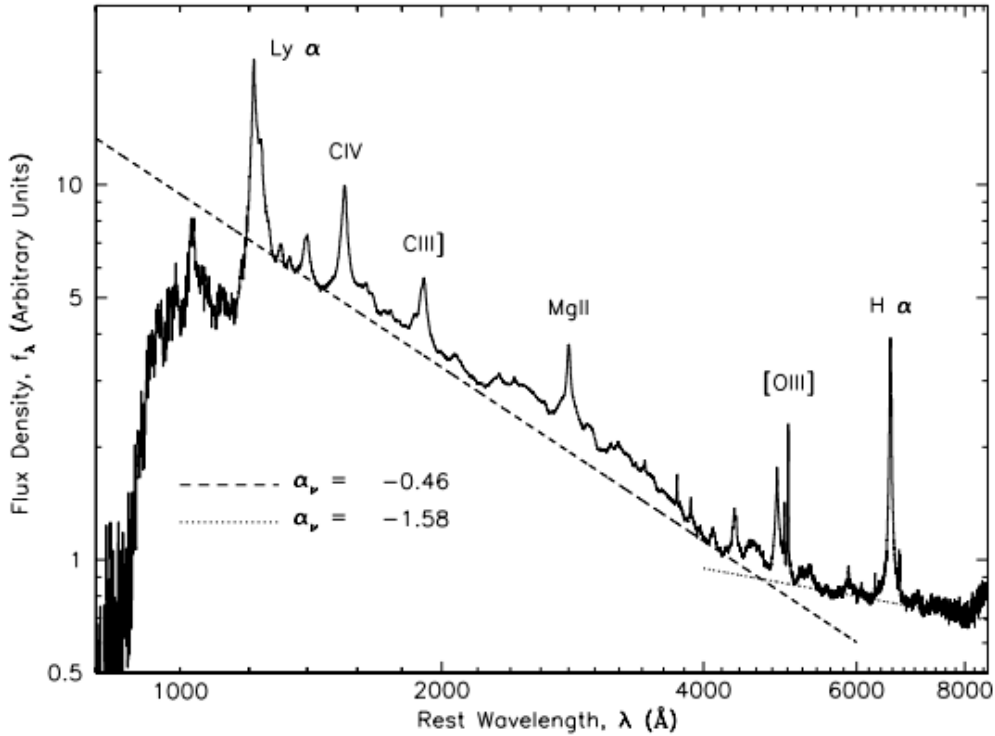


Figure 6: Composite stacked quasar spectrum from SDSS data taken from (Vanden Berk et al., 2001). Power-law fits to the estimated continuum flux from the data are plotted to accentuate the lines.

The typical spectral energy distribution (SED) of an accreting BH comprises weighted emission, which is produced by astrophysical processes occurring in distinct regions of the object — the accretion disk, the hot corona, and the surrounding dusty torus. The observed SED of an accreting BH spans all the way from the radio to very high-energy gamma-rays ($10^9 - 10^{30}$ Hz) and consists of a superposition of multiple components — a tall bump at high frequencies, a Black-Body component, and a plethora of emission and absorption lines (see Fig. 6 for the typical spectrum of a quasar in optical wavelengths; and Fig. 7 for the SED of an accreting BH over the entire range from radio to gamma ray wavelengths; further details of emission mechanisms and the corresponding scales on which they operate can be found in these two reviews, Netzer (2015); Peterson (2014)). Observed sources are organized primarily into two classes based on the width of emission lines in their spectra, a feature which tends to correlate with the viewing angle to the central BH. Type I AGN are characterized by the presence of relatively broad ($1000 - 20000 \text{ km s}^{-1}$) emission lines, which are produced by a population of the closely orbiting clouds that move in Keplerian orbits. Both these clouds and the accretion disk itself reside within the broad-line region (BLR), which can most readily be detected when the surrounding torus is viewed face-on. Type II AGN are characterized by the presence of narrow spectral emission lines ($300 - 1000 \text{ km s}^{-1}$), which originate from the more quiescent clouds that reside farther away from the accretion disk in the so-called narrow line region (NLR). When the galaxy is viewed edge-on, the obscuring dusty torus prohibits a direct view into the accretion disk, but permits a view of the toroidal region. Observed Type I AGN are more luminous than Type II AGN and therefore tend to comprise the bulk of observationally detected high-redshift sources. All optical quasars are Type I AGN and the thus far detected Type II AGN at $z \geq 3$ also have optical counter-parts. A population of heavily obscured Type II AGN that are as yet undetected are expected to exist across cosmic epochs and the high-redshift end population of these stands to be uncovered by JWST. For a more detailed description and illustration of these unified models, we refer the reader to these reviews and references therein (Netzer, 2015; Peterson, 2014). At present, we have a reasonably robust set of models that explain the origin of spectral data that are included in *QuasarNet*.

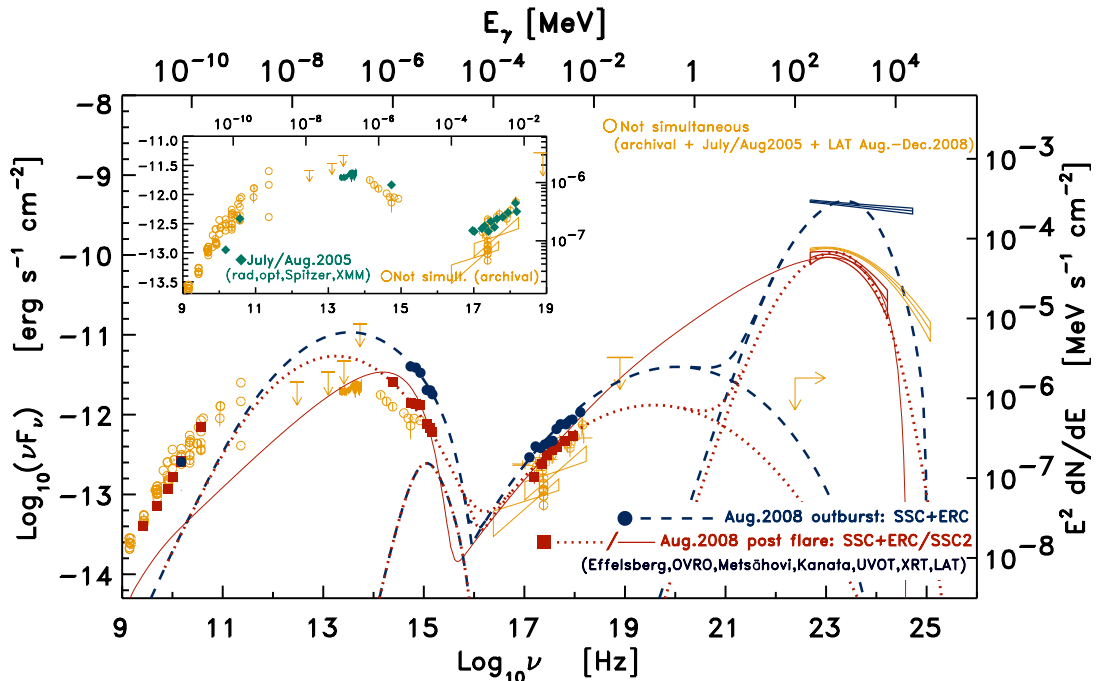


Figure 7: Major panel: Overall radio-to-gamma-ray spectral energy distribution (SED) of the quasar PKS 1502+106 assembled with data from the 2-week Fermi LAT multi-frequency campaign over-plotted with data from other multi-wavelength observatories in the radio, optical, X-ray and IR. Compilation published by the Fermi-LAT collaboration, from Fig. 11 of Abdo et al. (2010). The inset shows a zoomed in version of data from an earlier epoch.

4.7. Mass estimates for black holes

Mass and spin are fundamental properties of black holes. While mass estimates are available for several thousand sources (Kelly and Shen (2013); Peterson (2014); Vestergaard (2019)), at the present time, spin

measurements are available only for a handful of sources (Reynolds (2020); Nandra et al. (2006)). As the observed correlations are between SMBH mass and host galaxy properties, in this work, we restrict our investigation to BH masses. By construction the database structure of *QuasarNet* is kept inherently flexible to accommodate data on BH spins when they become available, at which time spins can be seamlessly incorporated to the other stored source attributes.

QuasarNet includes BH masses derived from multiple techniques. These include mapping the orbits of individual stars, which is possible only for the Milky Way (Genzel et al., 1997; Ghez et al., 1998); modeling the orbits of bulge stars from imaging and spectroscopy as performed for nearby galaxies (Tremaine et al., 1994) and using measurements of the speed of rotating gas using water mega-masers as tracers of the mass (Miyoshi et al., 1995). It has been demonstrated that the luminosity of an accreting SMBH can be used to infer its BH mass across a range of redshifts.

One widely adopted method for SMBH mass determination, assumes that the BLR is virialized and that the motion of the emitting clouds reflects the gravitational potential of the central BH Blandford and McKee (1982); Peterson (1993). Under this assumption, the black hole mass M_{\bullet} can be estimated via:

$$M_{\bullet} = f \frac{V_{\text{vir}}^2 R_{\text{BLR}}}{G}, \quad (2)$$

where V_{vir} is the virial velocity, R_{BLR} is the size of the BLR, G is Newton's gravitational constant, and f is the virial coefficient that accounts for the geometry and kinematics of the material around the BLR (Shen, 2013). The virial velocity can be estimated using the velocity dispersion derived from the width of observed BLR emission lines. The time-lagged broad-line response to variations in the continuum flux enables the measurement of the light travel time from the central ionizing source to the broad line regions, which can be used to estimate R_{BLR} . Acquiring these time lags from reverberation data is challenging, as it requires a long observational baseline, monitoring an accreting BH for six months to a year (Peterson et al., 2004; Grier et al., 2017). In *QuasarNet*, we include BLR determined masses and errors therein where available. There are many interesting questions relevant to observed variable quasars, like the sources referred to as "changing look" quasars. However for these, uniform sampled variability data are not currently available and are hence not included in *QuasarNet*.

An alternative method for SMBH mass measurements, that is not predicated on the assumption of virialization of the BLR, is one in which line and continuum luminosities from the X-ray, ultraviolet, infrared, and optical wavelengths can instead be used to estimate the BLR size. For this purpose, continuum luminosities L_{cont} are often preferred over line luminosities, because they tend to yield a tighter correlation with the size of BLR (Kaspi et al., 2000, 2005; Bentz et al., 2009). Reverberation mapping has revealed a tight correlation between the size of BLR and the continuum luminosity. This empirical scaling relationship is then used to derive black hole mass. Therefore, the continuum luminosity L , combined with the widths of broad emission lines (Δv), can be used to derive estimates of the mass of the black hole:

$$\log \left(\frac{M_{\bullet}}{M_{\odot}} \right) = a + b \log \left(\frac{L}{L'} \right) + c \log \left(\frac{\Delta v}{\Delta v'} \right), \quad (3)$$

where $L' = 10^{44} \text{ erg s}^{-1}$, $\Delta v' = 1 \text{ km s}^{-1}$. In general, the values of pre-factors a and b depend on the choice of the luminosity and velocity dispersion estimators, and if a virialized BLR is assumed, then the coefficient of the line width is typically taken to be $c = 2$ (Shen and Liu, 2012). Various cross-calibrations for this relation have been proposed (Shen and Liu, 2012; Vestergaard and Peterson, 2006; Vestergaard and Osmer, 2009; Trakhtenbrot and Netzer, 2012). Additional calibrations are needed to reconcile with estimates from other methods (Coatman et al., 2017) and for the determination of robust error-bars. For example, the masses derived using the continuum luminosity are often calibrated with BH mass measurements obtained from reverberation mapping. Additional BH mass estimates are often made using individual lines like the Carbon-IV lines (Vestergaard and Peterson, 2006) as seen in the SED template of Fig. 6. In *QuasarNet* we compile all available BH mass estimates as shown in the schematic (Fig. 1) into the Quasar Spectra Table, computing them when relevant measured quantities are available. We also keep track of the error bars in the mass estimates when available. The Black Hole Mass Function (BHMF) is a key component of theoretical models. Apart from the study of individual objects, population studies of quasars can reveal aspects of their evolution across multiple cosmic epochs and are crucial for building evolutionary models. Large quasar samples derived from ambitious astronomical surveys have enabled the study of the cosmological evolution of the quasar luminosity function (QLF). A critical quantity for theoretical modeling, the QLF, encapsulates the growth history of quasars through accretion. The importance of the QLF was demonstrated in early modeling work, and it continues to be

vigorously studied in the field (for example see early work by (Small and Blandford, 1992; Haehnelt et al., 1998; Hasinger, 2008)). The two observationally derived quantities that drive theoretical modeling are the BHMF and QLF. The *QuasarNet* database by design permits easy computation of both the QLF and BHMF as demonstrated in the workflow examples in the main paper.

The QLF is one of the key inputs to current conceptual models of BH growth (see reviews that outline the methodology by Volonteri (2012); Natarajan (2014) and references therein). The specifications of observational surveys needs to be taken into account to determine the QLF. Observationally determined QLFs are then compared with those predicted by theoretical models of BH growth. Calibrated with data, the honed models are extrapolated and then used to predict QLFs down to fainter luminosities than observed limits and out to larger redshifts than current detections. The most recent predicted QLFs extrapolated to a wider range than currently available observations computed as a function of redshift out to $z = 9$ can be found in Ricarte and Natarajan (2018b)). The QLF provides a census of the number of sources at a given redshift and absolute magnitude M . It is computed as follows:

$$\phi(M, z) \approx \sum_{j=1}^N \frac{1}{V_a^j} (\Delta M)^{-1}, \quad (4)$$

where ΔM is magnitude range $\{M, M + dM\}$, and V_a^j is the effective volume for a source j . This is usually estimated with the binned-volume method (Avni and Bahcall, 1980), where the effective volume is estimated using:

$$V_a^j = \int_M^{M+\Delta M} \int_{\Omega} \int_{z_{min}}^{z_{max}} dM dz f(M, z) \frac{dV}{dz d\Omega}, \quad (5)$$

where $f(M, z)$ is the survey sample completeness, z_{min} and z_{max} define the redshift bin over which the QLF is averaged, $\frac{dV}{dz d\Omega}$ is the comoving volume element, and $d\Omega$ is the survey area. The minimum z_{min} is determined by the specifications of the survey. The maximum redshift z_{max} depends on individual sources and is defined by the maximum redshift out to which the source would remain detectable given the survey detection limit, as specified by the selection function of the survey. *QuasarNet* collates data for computing the QLF by merging observations taken by several independent surveys while keeping track of the selection function of the surveys - these are stored in the Quasar Photometry Table (see the schematic in Fig. 1.

5. Current Data Landscape

For studies of BHs, the data landscape of interest for us comprises both simulations and observations — each of which are growing in size and complexity. Simulations spanning various physical scales ranging from Magneto-hydrodynamic simulations (MHD) of the gas inflow and dynamics on sub-pc scales to cosmological simulations that track the fate of gas flowing in from the larger-scale cosmic web are currently available. Varying in detail and complexity, these simulations now also include the physics of the formation of stars in galaxies and feedback effects driven by the SMBHs, as briefly outlined below.

5.1. Observational Data

In this section, we first discuss multi-wavelength observational data, including extant data archive facilities, their content and how they are currently configured for access and use before outlining the specific sources that we use to construct *QuasarNet*. Both space-based and ground-based observatories have been essential for developing a multi-wavelength picture of central SMBHs. For example, data from HST, Chandra, XMM, Herschel, and Spitzer Space Telescopes spanning X-ray to infrared wavelengths, and their cross-correlations have revealed important ways in which BH accretion is related to key host galaxy properties like stellar mass and star formation rate (Chen et al., 2013)). Most space missions and ground-based observational surveys have been efficiently cataloging their own data to permit public access after the lapse of the data proprietary period. One important challenge in dealing with quasar data pertains to how candidates are traditionally selected from surveys, using color-color diagnostics via the drop-out technique (originally developed to extract high-redshift galaxies) that exploits the spectral shape of their SEDs per templates shown in Figs. 1 & 2 (Steidel et al. (1999)). Therefore, at progressively higher redshifts only the most luminous quasars are detected, making it difficult to detect and discern properties of fainter sources. This is precisely where we see the power of ML techniques that

will enable extrapolation of the detected sample by predicting the properties of hitherto undetected fainter sources based on sources currently seen.

HST has acquired data on many quasars and their galaxy hosts over more than three decades of operation. This data is efficiently archived in and distributed from the Mikulski Archive for Space Telescopes (MAST) hosted and managed by the Space Telescope Science Institute ⁸. In addition to the images - raw, cleaned, and processed - MAST provides high-level science-ready data products. In particular, MAST houses the AGN SED ATLAS Brown et al. (2019), which contains the full SEDs of 41 AGN at present, derived from multi-wavelength photometry and archival spectroscopy, that combines information from eight MAST-supported projects (HST, SWIFT-UVOT, GALEX, PanSTARRS, IUE, FUSE, HUT, WUPPE) plus an additional nine other missions/observatories. Beyond this Atlas, MAST also contains 80 SEDs of accreting sources, composites that are produced by mixing the SEDs of the central regions of active sources with their host galaxy SEDs. This high-level science products database contains a total of 121 AGN whose SEDs span a wavelength range from $\sim 0.09 - 30.0$ microns. For some sources, additionally, there is even broader wavelength coverage extending into the X-ray, far-infrared, and radio ⁹. The archival data is stored in relational database tables, which are accessed through two user interfaces — a Java-based application (“StarView”) and a web-based application: neither of these require the user to understand the database architecture or how to use Structured Query Language (SQL) to browse and extract data.

The ground-based Sloan Digital Sky Survey (SDSS) has mapped a third of the sky and provides the most detailed three-dimensional data for more than three million unique astronomical objects ¹⁰. SDSS contains more than half a million quasars detected out to $z \sim 7$ and comprises a homogeneous sample of quasars with optical spectra. Each round of the SDSS quasar surveys was motivated by a different science goal. For example, the SDSS DR7 quasar catalog consists of 105,783 spectroscopically confirmed quasars from the SDSS-I/II survey whose aim was to study the quasar luminosity function and their clustering properties Abazajian et al. (2009). With every data release, the number of detected quasars has grown dramatically. The latest SDSS DR14, not only increased the number of quasars by a factor of five compared to the SDSS DR7, it also went 1.5 magnitudes fainter, enabling the probing of quasar properties over a much larger luminosity range Abolfathi et al. (2018). Though the SDSS catalogs contain the X-ray, UV, optical, IR and radio imaging properties of the quasars wherever available, they lack spectral information for the majority of sources. Spectra have been obtained from detailed follow-up studies. The detection of quasars and their redshift estimates are done primarily using the color-color selection of drop-outs (Richards et al. (2002)). The SDSS archive also offers a range of sophisticated science products that are available as Value Added Catalogs (VAC) ¹¹. The publicly available resource that we utilize to collect data for *QuasarNet* is the NASA-IPAC Extra-galactic Database (NED)¹². This database contains basic information — e.g., coordinates and magnitude — on all observed astronomical objects and references to all published papers that describe the sources, and this includes reports of detailed follow-up work. Unlike other archives like the MAST, SDSS and SDSS VAC, the NED repository does not contain customized value added properties, however, it contains the most comprehensive compilation of publication references for surveys and follow-up studies and is consistently updated. It is this feature of NED that we deploy for *QuasarNet* the comprehensive bibliographic data. Due to the plethora of new observatories and instruments on the ground and in space due to come online soon, we are entering an era of an unprecedented deluge of multi-wavelength and multi-messenger data on active and dormant BHs. From the ground, the Vera Rubin Observatory’s projected output catalog is expected to provide 15 petabytes of data over 10 years of operation (Jurić et al., 2017). The targeted AGN Survey, in particular, is expected to uncover $N \sim 10^7$ optical quasars (LSST Science Collaboration et al., 2009). JWST, planned for launch in 2021¹³, has instruments with sensitivity in the mid-, near- and far-infrared wavelength (ranging from $\sim 1 - 30$ microns), that will open up an entirely new window into the early universe, revealing populations of early BHs and the first galaxies (Pacucci et al., 2016; Natarajan et al., 2017; Barrow et al., 2018). The planned Laser Interferometer Space Antenna (LISA) mission¹⁴ to be launched in the early 2030’s also offers exciting prospects for detecting gravitational

⁸https://archive.stsci.edu/hst/search_retrieve.html

⁹<https://archive.stsci.edu/hlsp/index.html>

¹⁰https://www.sdss.org/dr16/data_access/

¹¹https://www.sdss.org/dr14/data_access/value-added-catalogs/

¹²<https://ned.ipac.caltech.edu>

¹³<https://www.jwst.nasa.gov/>

¹⁴<https://www.elisascience.org/>

waves from binary SMBH mergers that will most likely be accompanied by multi-wavelength electromagnetic counter-parts (Colpi et al., 2019; Taylor et al., 2019; Kelley et al., 2018; Katz et al., 2020). Other relevant facilities providing new data on BHs include the Canadian Hydrogen Intensity Mapping Experiment (CHIME)¹⁵; the soon to be launched NGRST¹⁶; the Euclid Space Mission¹⁷; the Square Kilometer Array (SKA)¹⁸; the Next Generation CMB Experiment Stage 4 (CMB-S4)¹⁹, and the Advanced Telescope for High-ENergy Astrophysics (ATHENA)²⁰.

5.2. Simulated Data

Used together, observations and numerical simulations have enabled detailed studies of many aspects of BH physics, including the accretion process, feedback from growing BHs, the evolution of the black hole population and how BHs fit into the larger picture of structure formation in the Universe as demonstrated in Springel et al. (2005b). The power of simulations lies in the density of information that can be mined from them for all constituent particles - dark matter, baryons and BH sink particles that enable connecting physical scales, and regimes across cosmic epochs. Simulations also place BH growth in its full astrophysical context against the backdrop of dark matter driven galaxy formation. Simulations have shown that the energy released from the accretion process has the capacity to impact a wide range of spatial scales — from the smallest scales where general relativity and magneto-hydrodynamic processes dominate to the largest scales wherein outflows driven by accreting black holes and their feedback are relevant (Beskin and Kuznetsova, 2000; Komissarov, 2001; Gammie et al., 2003; Komissarov, 2005; McKinney, 2005; Harrison et al., 2018; Phipps et al., 2020). This coupling of scales might hold the key to understanding the observed correlations. Due to the complexity of the involved physics and numerical cost of ab-initio simulations of BH formation and subsequent evolution, simulators have adopted a strategy in which they focus on specific aspects of the problem. For instance, in a given simulation suite, they follow a subset or all of the relevant physics involved such as gravity, hydrodynamics (e.g. Beckmann et al., 2018), magneto-hydrodynamics and radiation transfer (McKinney, 2005; Hawley et al., 2007; Tchekhovskoy et al., 2011; Liska et al., 2018). Besides this, they need to account for the initial conditions for forming/seeding BHs and the level of detail with which the environment around them is rendered. Combining information from different simulations has allowed us at present to build a consistent picture spanning a large range of length scales. Take for example, the role of jets driven by BHs, Tchekhovskoy et al. (2010) use small scale general relativistic magneto-hydrodynamic simulations to investigate the connection of the BH spin to the power of radio-emitting jets. Complementary simulations by Gaibler et al. (e.g. 2011) bridge the gap to larger spatial scales and look at the impact of jets on galactic discs in Newtonian hydrodynamical simulations. This permits assessing the impact of jets on the provision of fuel for the growing BH and the global star formation in the host galaxy. The latter simulations use idealised initial conditions for their setup and neglect the impact of feedback on the gas in the immediate vicinity of the central BH. Lower resolution cosmological zoom simulations on the other hand are able to resolve individual objects such as the dark matter halos that host BHs with spatial resolutions of up to tens of pc (e.g. Debuhr et al., 2011) and at the same time keep track of the cosmological environment and its coupling with the BH (e.g. Beckmann et al., 2019). These simulations not only track BH relevant physics but also follow the evolution of the host galaxy in terms of its star formation, metal enrichment and feedback from exploding supernovae (e.g. Beckmann et al., 2019; Wise et al., 2019; Latif and Khochfar, 2020). The ever-increasing number of observed BHs and AGN require numerical simulations to span a large parameter space of initial conditions for the formation of BHs and their cosmic environment. This goes beyond what current zoom simulations can computationally provide. As quasars and AGN are extremely rare objects, rare compared to galaxies in the cold dark matter driven Universe, simulations in which their formation and growth are tracked self-consistently over cosmic time are extremely computationally challenging. To account for this, trade-offs are often made between the simulation volume and resolution. For example, large scale cosmological simulations of cosmic volumes of $\sim (100 \text{ Mpc})^3$ with coarser spatial resolution of $\sim \text{kpc}$ (e.g. Schaye et al., 2015) have been performed. These simulations typically include sub-grid models for the baryonic physics i.e. star formation, cooling of gas, chemical networks, stellar population evolution, supernovae feedback, and metal enrichment tracked via

¹⁵<https://chime-experiment.ca/>

¹⁶<https://roman.gsfc.nasa.gov/>

¹⁷<https://sci.esa.int/web/euclid>

¹⁸<https://www.skatelescope.org/>

¹⁹<https://cmb-s4.org/>

²⁰<https://sci.esa.int/web/athena>

radiative transfer but can only include limited BH physics (Di Matteo et al., 2005; Robertson et al., 2006; Sijacki et al., 2007; Debuhr et al., 2011; Vogelsberger et al., 2014; Schaye et al., 2015; Sijacki et al., 2015; Habouzit et al., 2017; Weinberger et al., 2018). To match the statistical properties of AGNs in large observational surveys yet larger scale simulations with volume $> (500 \text{ Mpc})^3$ are needed (e.g. Bower et al., 2006). Given current computational limits, such simulations have necessarily been dark matter only and are able to only incorporate simplified, analytic models for the physics of BHs and galaxies. *QuasarNet* offers a novel way to associate observed BHs with their putative host galaxies and dark matter halos in co-eval simulated slices. We demonstrate one example of the kind of novel association study that *QuasarNet* allows us to pursue in tracking the potential assembly history of the dark matter halos that hosts an observed $z = 3$ quasar, shown in Fig. 2 of the main paper. ML tools that we plan to develop in the next stage of our project will allow us to further mimic larger simulated volumes that correspond to observational survey volumes and predict the putative locations for fainter as yet undetected quasars. Here we present the first key step in building up BH-galaxy-halo connection that underpins the formation and evolution of all structures including the non-baryonic (dark matter), baryonic (galaxies) and BHs. Over the last two decades with the advent of powerful computational architectures, the size of data and complexity of numerical simulations has significantly increased. Typical data sets are of Terabyte size and contain $N > 1024^3$ computational elements that represent gas, stars, black holes and dark matter. For each of these elements, the equation of motion is solved taking into account the full physical information available in the simulation. Besides containing phase-space information on momentum and spatial coordinates, computational elements also carry further information to compute the evolution of the system in time such as e.g. the spin and mass of black holes, chemical composition of gas and stars, the present mass function of stars that is associated with an individual star particle and internal energy and density of gas. In addition, it has become practice to add evolutionary information to elements that is needed for sub-grid computations during the simulation or post-processing of the data. These include the birth age of a star particle to track the evolutionary state of the underlying stellar population that it represents or the maximum temperature an individual gas element achieved during its evolution, to name just a few. It is evident that this list could be arbitrarily expanded putting pressure on resulting data volumes. On top of this, simulation data sets include frequent snapshots with the full information of the state of all constituents - dark matter, stars and BHs - and their evolution through time. Further dramatic increase in data volumes is expected over the next decade with new peta-scale codes that will increase the number of computational elements significantly. To deal with such large data volumes the optimal strategy is to focus on only a subset of the information. In our case, we are concerned with BH formation and evolution which takes place in gravitationally bound dark matter halos. Focusing only on material bound to dark matter halos reduces the data volume to roughly $\sim 20 - 30\%$. One way to identify dark matter halos is based on linking dark matter particles by assuming a fixed linking length that is a fraction $b = 0.2$ times the mean inter-particle separation (Davis et al., 1985). These so-called Friends-of-Friends (FOF) halos contain further sub-structure in form of sub-halos that contain galaxies and BHs. Several different approaches have been utilised in the literature to identify subhalos based on their being gravitationally self-bound (e.g. Springel et al., 2001; Behroozi et al., 2013). Halo catalogues have become the standard way of providing the information from cosmological simulations to the community. They store all the relevant information on collapsed halos; global properties of dark matter halos (e.g. total mass and angular momentum), those of their constituent galaxies (e.g. star formation rate and metallicity) and BH (e.g. mass, accretion rate and spin). This set is complemented by information on all the gas, stars, BH and dark matter in the region defined by the halo. Halo catalogues are easily ingested in SQL databases (e.g. Millennium simulation Springel et al. (2006)²¹, Illustris simulation (Nelson et al., 2015)²² or the EAGLE project (Schaye et al., 2015)²³) which allow easy and fast access for population studies. A complementary approach is to use a web-based Application Programming Interface (API) which allows for in depth analyses of data beyond halo catalogues without the need of storing a local copy. Within *QuasarNet* we provide simulation data using a combination of these approaches to maximize the ease of application for ML techniques. For this pilot project, we first focus on dark matter only simulations and collate simulated halo properties into the Halo properties Table in *QuasarNet*.

²¹<https://www.g-v-o.org>

²²<https://www.illustris-project.org>

²³<http://icc.dur.ac.uk/Eagle/database.php>

z Range	Num. Quasars	Luminosity Estimator	Vel. Disp. Estim.	Reference
3.01-4.33	43	$L_\lambda(1350), L_\lambda(3000),$ $L_\lambda(5100), L(H\beta), L(MgII),$	$H\beta, Mg II, C IV$	Shen et al. (2019a)
3.00-5.46	7955	$L_\lambda(1350), L_\lambda(3000),$ $L_\lambda(5100), L(H\beta), L(MgII)$	$H\beta, Mg II, C IV$	Shen et al. (2011)
3.00-4.89	26571	$L_\lambda(1350), L_\lambda(3000), L_\lambda(5100)$	$Mg II, C IV$	Kozłowski (2017)
3.22-3.76	24	$L_\lambda(3000), L_\lambda(5100)$	$H\beta, Mg II$	Zuo et al. (2015)
4.52-6.41	21	$L_\lambda(3000)$	$Mg II$	De Rosa et al. (2011)
4.66-4.92	40	$L_\lambda(1450), L_\lambda(3000)$	$Mg II$	Trakhtenbrot et al. (2011)
5.64-6.42	50	$L_\lambda(1350), L_\lambda(1700), L_\lambda(3000)$	$Mg II, CIV$	Shen et al. (2019b)
5.77-6.31	6	$L_\lambda(1350), L_\lambda(3000)$	$Mg II, CIV$	Jiang et al. (2007)
5.82-6.28	5	$L_\lambda(1350), L_\lambda(3000)$	$Mg II, CIV$	Kurk et al. (2007)
5.90	1	$L_\lambda(3000)$	$Mg II$	Eilers et al. (2018)
5.98-6.44	9	$L_\lambda(3000)$	$Mg II$	Willott et al. (2010a)
6.13	1	$L_\lambda(3000)$	$Mg II$	Shao et al. (2017)
6.48-7.08	11	$L_\lambda(3000)$	$Mg II$	Mazzucchelli et al. (2017)
6.60-7.10	4	$L_\lambda(3000)$	$Mg II, CIV$	De Rosa et al. (2014)
7.07	1	$L_\lambda(1350)$	$Mg II$	Matsuoka et al. (2019)

Table 1: The compiled list of quasars including additional properties of the supermassive black holes included in our database. This table comprises data from reported spectroscopic measurements of individual quasars.

z range	Survey	Reference	Number of quasars	Area (deg ²)
2.2–3.5	BOSS DR9	Ross et al. (2013)	23301	2236.0
3.7–4.7	SDSS DR7	Schneider et al. (2010)	1785	6248.0
3.6–5.2	NDWFS	Glikman et al. (2011)	12	1.71
3.8–5.3	DLS	Glikman et al. (2011)	12	2.05
4.7–5.4	SDSS+WISE	Yang et al. (2016)	99	14555.0
4.7–5.5	SDSS DR7	McGreer et al. (2013)	103	6248.0
4.7–5.5	— Stripe 82	McGreer et al. (2013)	59	235.0
5.7–6.5	SDSS Main	Jiang et al. (2016)	24	11240.0
5.7–6.5	— Overlap	Jiang et al. (2016)	10	4223.0
5.7–6.5	— Stripe 82	Jiang et al. (2016)	13	277.0
5.8–6.6	CFHQS Deep	Willott et al. (2010b)	1	4.47
5.8–6.6	— Very Wide	Willott et al. (2010b)	16	494.0
5.8–6.5	Subaru High- z Quasar	Kashikawa et al. (2015)	2	6.5
4.0–6.5	CANDELS GOODS-S	Giallongo et al. (2015)	19	0.047
6.5–7.4	UKIDSS	Mortlock et al. (2011)	1	3370.0
6.5–7.4	UKIDSS	Venemans et al. (2015)	1	3370.0
6.5–7.4	ALLWISE+UKIDSS +DECaLS	Bañados et al. (2018)	1	2500.0

Table 2: The list of quasar survey samples that are included in our database and *QuasarNet* research portal.

Name	Units	Description
z	-	redshift
M_{vir}	M_\odot	virial mass
r_{vir}	kpc	virial radius
x, y, z	Mpc	position
v_x, v_y, v_z	km s^{-1}	peculiar velocity
J_x, J_y, J_z	$M_\odot \text{ Mpc km s}^{-1}$	angular momentum
\dot{M}_{acc}	M_\odot/yr	accretion rate onto halo
I_{desc}	-	descendant halo ID
$T/ U $	-	virial parameter
x_i, y_i, z_i	Mpc	position of each particle
$v_{x,i}, v_{y,i}, v_{z,i}$	km s^{-1}	peculiar velocity of each particle

Table 3: Examples of dark matter halo properties stored in *QuasarNet*.

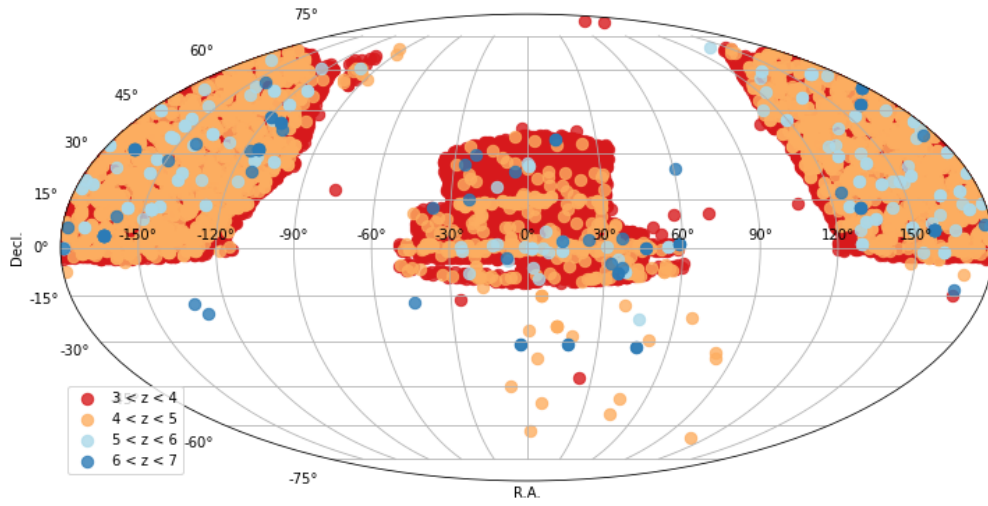


Figure 8: The distribution of quasars collated in *QuasarNet* on the sky. Sources are color-coded according to their redshifts: $3 < z < 4$ - orange; $4 < z < 5$ - blue; $5 < z < 6$ - cyan and $6 < z < 7$ - pink.

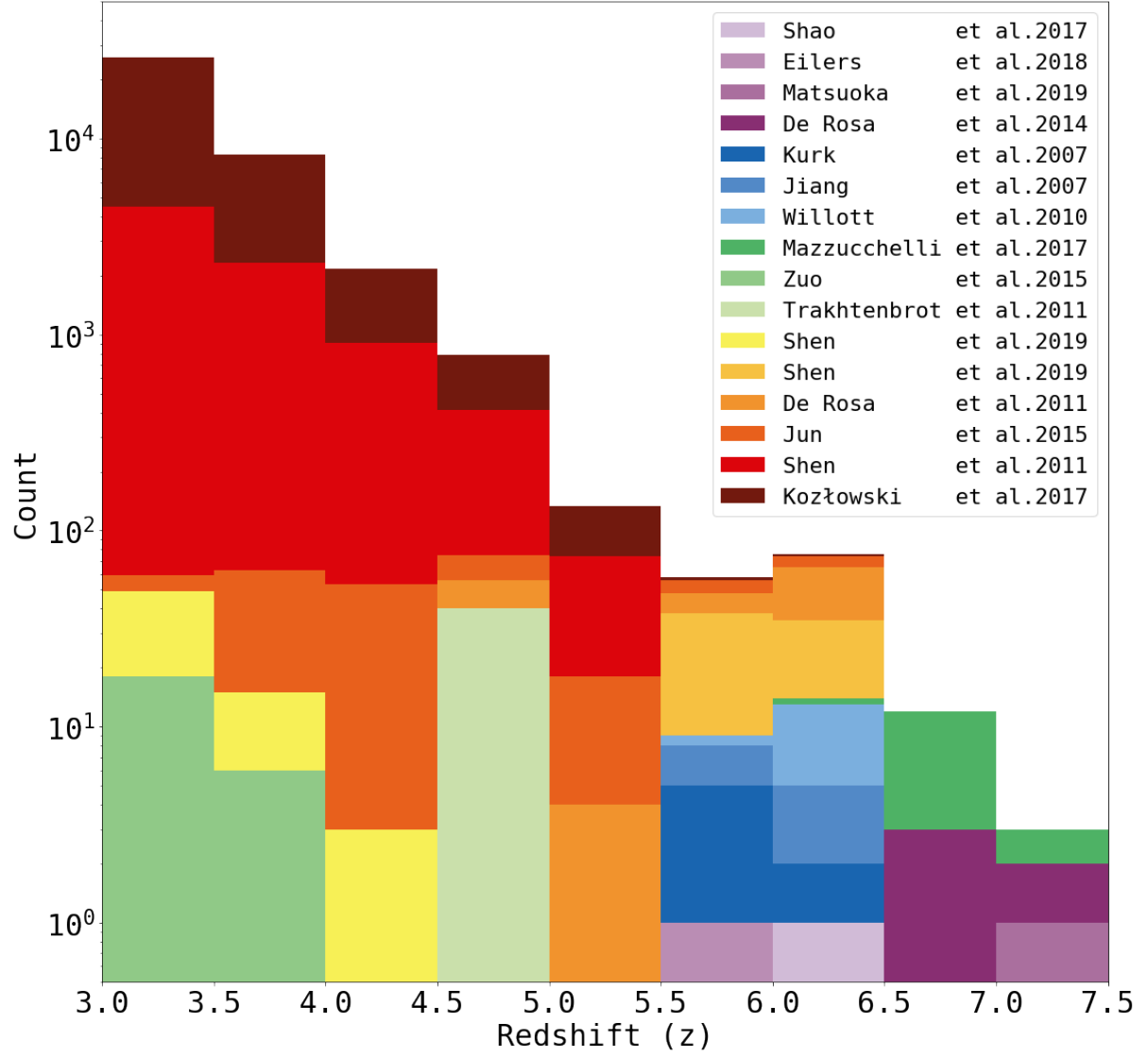


Figure 9: BH/Quasar Population Demographics: The number of quasars plotted as a function of redshift collected from various sources (referenced in the inset) from the Quasar Spectra data table of *QuasarNet*.

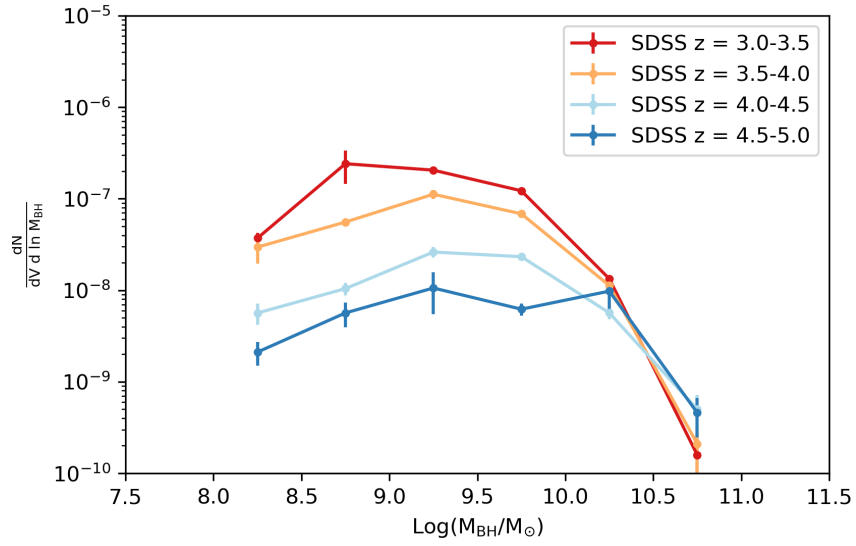


Figure 10: The black hole mass function – an important quantity for calibrating/constraining theoretical models of black hole mass assembly and growth can be derived from the collated tables in *QuasarNet* and swiftly plotted. Here we plot the BHMF as a function of redshift queried from *QuasarNet* derived from the SDSS survey (SDSS DR7 for the $z < 5$ quasars).